






The phenotype of the most common human ADAR1p150 Z α mutation P193A in mice is partially penetrant

Zhen Liang^{1,2} , Alistair M Chalk^{1,2} , Scott Taylor¹ , Ankita Goradia¹, Jacki E Heraud-Farlow^{1,2,*}  & Carl R Walkley^{1,2,*} 

Abstract

ADAR1-mediated A-to-I RNA editing is a self-/non-self-discrimination mechanism for cellular double-stranded RNAs. ADAR mutations are one cause of Aicardi-Goutières Syndrome, an inherited paediatric encephalopathy, classed as a “Type I interferonopathy.” The most common ADAR1 mutation is a proline 193 alanine (p.P193A) mutation, mapping to the ADAR1p150 isoform-specific Z α domain. Here, we report the development of an independent murine P195A knock-in mouse, homologous to human P193A. The *Adar1*^{P195A/P195A} mice are largely normal and the mutation is well tolerated. When the P195A mutation is compounded with an *Adar1* null allele (*Adar1*^{P195A/-}), approximately half the animals are runted with a shortened lifespan while the remaining *Adar1*^{P195A/-} animals are normal, contrasting with previous reports. The phenotype of the *Adar1*^{P195A/-} animals is both associated with the parental genotype and partly non-genetic/environmental. Complementation with an editing-deficient ADAR1 (*Adar1*^{P195A/E861A}), or the loss of MDA5, rescues phenotypes in the *Adar1*^{P195A/-} mice.

Keywords ADAR1; A-to-I RNA editing; MDA5; P193A mutation; Z α domain

Subject Categories Molecular Biology of Disease

DOI 10.15252/embr.202255835 | Received 21 July 2022 | Revised 13 February 2023 | Accepted 28 February 2023 | Published online 28 March 2023

EMBO Reports (2023) 24: e55835

Introduction

One of the most common RNA modifications in mammals is the deamination of adenosine to inosine, termed A-to-I editing, in double-stranded regions of RNA (dsRNA) by adenosine deaminase acting on RNA 1 (ADAR1) and ADAR2 (Eisenberg & Levanon, 2018). A-to-I editing results in the non-reversible conversion of adenosine to inosine for the targeted nucleotide within RNA. Inosine is usually interpreted as guanosine during translation. Depending on

where the editing site lies in the transcript A-to-I editing can have a variety of consequences (Solomon *et al.*, 2013, 2017; Walkley & Li, 2017; Eisenberg & Levanon, 2018). Editing within protein-coding sequences can change the amino acid codon, and therefore the protein product, from that genomically encoded (Licht *et al.*, 2019). A-to-I editing can also impact RNA splicing, stability, translation, and localisation (Lev-Maor *et al.*, 2007; Shoshan *et al.*, 2015; Stellos *et al.*, 2016; Kapoor *et al.*, 2020) as well as the biogenesis of non-coding RNAs (microRNAs (Kawahara *et al.*, 2007) and circRNAs (Ivanov *et al.*, 2015)). Editing alters the base-pairing properties within RNA, both stabilising and destabilising the RNA secondary structure depending on context (Liddicoat *et al.*, 2015; Solomon *et al.*, 2017). A-to-I editing can be readily detected using sequencing methods, as A-to-I editing can be identified by A-to-G mismatches between the cDNA and genomic DNA, allowing genome-wide mapping (Levanon *et al.*, 2004; Li *et al.*, 2009; Ramaswami *et al.*, 2013).

There are millions of A-to-I editing sites across all tissues within the human transcriptome, with the majority located in repetitive elements such as *Alu* repeats (Bazak *et al.*, 2014; Picardi *et al.*, 2015; Tan *et al.*, 2017; Gabay *et al.*, 2022). In mice, there are between 50,000 and 150,000 editing events, also concentrated in evolutionarily related repetitive elements (SINE/LINEs) (Pinto *et al.*, 2014; Pfaller *et al.*, 2018; Licht *et al.*, 2019; Costa Cruz *et al.*, 2020). The key physiological function of ADAR2 is to recode the *Gria2* transcript by editing a coding region of the mRNA, resulting in an amino acid substitution and a correctly functioning GluA2 protein (Higuchi *et al.*, 1993, 2000). In contrast to the recoding of a single mRNA target for ADAR2, it has been demonstrated by multiple groups that the physiologically most important function of ADAR1 editing is to prevent the cells' own RNA from being mistaken as foreign RNA by the innate immune system (Mannion *et al.*, 2014; Liddicoat *et al.*, 2015; Pestal *et al.*, 2015). ADAR1's primary physiological function is to counteract cytoplasmic innate immune sensing by melanoma differentiation-associated protein 5 (MDA5) of endogenous RNAs (Hartner *et al.*, 2009; Liddicoat *et al.*, 2015; Heraud-Farlow *et al.*, 2017; Chalk *et al.*, 2019), a species conserved function (Pestal *et al.*,

1 St Vincent's Institute of Medical Research, Fitzroy, Vic., Australia

2 Department of Medicine, Eastern Hill Precinct, Melbourne Medical School, University of Melbourne, Fitzroy, Vic., Australia

*Corresponding author. Tel: +61 3 9231 2480; E-mail: jhfarlow@svi.edu.au

**Corresponding author. Tel: +61 3 9231 2480; E-mail: cwalkley@svi.edu.au

†These authors contributed equally to this work

2015; Chung et al, 2018). ADAR1 is expressed as two isoforms, a constitutive and primarily nuclear p110 protein and an inducible and mostly cytoplasmic p150 isoform. Recent studies have focussed attention on the role of the cytoplasmic p150 isoform and how this intersects with innate immune sensing (Ward et al, 2011; Pestal et al, 2015; Kim et al, 2021).

ADAR (ADAR1) loss-of-function mutations have been identified as one of the genetic causes of Aicardi-Goutières Syndrome (AGS) (Rice et al, 2012, 2017). AGS is an inherited paediatric encephalopathy, classed as an auto-inflammatory “Type I interferonopathy,” characterised by the upregulation of interferon (IFN) and interferon-stimulated gene (ISG) expression (Crow & Manel, 2015). AGS patients with ADAR mutations most often have compound heterozygous mutations, with one mutation impacting the p150 isoform together with a second that affects both p110 and p150 isoforms (Rice et al, 2012, 2017). Mutations in ADAR have also been identified in bilateral striatal necrosis (BSN), where patients have a dystonic or rigid movement disorder associated with symmetrical abnormalities of the brain (Livingston et al, 2014). Similar to ADAR mutant AGS, BSN patients with ADAR mutation have a characteristic “interferon signature.” Recent knock-in mouse models have begun to address how distinct ADAR1 mutations, including those reported in AGS and BSN, impact the function of ADAR1 *in vivo* (de Reuver et al, 2021; Guo et al, 2021; Inoue et al, 2021; Maurano et al, 2021; Nakahama et al, 2021; Tang et al, 2021).

The most frequently reported ADAR1 mutation is proline 193 to alanine (p.Pro193Ala; P193A; Rice et al, 2017), which maps to the unique Z α domain of the p150 isoform (Herbert et al, 1995, 1998; Herbert & Rich, 2001; Herbert, 2021; Nakahama & Kawahara, 2021). The Z α domain is found in only one other protein in the human genome, Z-DNA-binding protein 1 (ZBP1), that activates cell death pathways during viral infection (Newton et al, 2016; Jiao et al, 2020; Zhang et al, 2020). Proline 193 contacts the left-handed helix structure characteristic of Z-form DNA and RNA and is important in the interaction between ADAR1p150 and Z-form nucleic acid (Schwartz et al, 1999). Interestingly, unlike other ADAR mutations, the P193A mutation is present at an allele frequency of 0.002 of the human population globally (Herbert, 2020; Karczewski et al, 2020), however, the effects of this mutation are not definitively understood. In human populations, the P193A mutation is nearly always heterozygous (Karczewski et al, 2020). Maurano et al (2021) recently reported the development and characterisation of a murine p.Pro195Ala (P195A) mutant mouse model, homologous to the human P193A mutation. They reported that the P195A allele was well tolerated in isolation and was homozygously viable with a normal lifespan. When combined with a second mutation, either a p110/p150-deficient allele or p150 null allele, they reported a completely penetrant shortened lifespan and reduced weaning weights, with evidence of activation of an innate immune/interferon and integrated stress response gene expression program in the *Adar1*^{P195A/p150}. They report rescue of the phenotypes by loss of MDA5 consistent with prior genetic rescue of ADAR1 loss-of-function alleles (Liddicoat et al, 2015; Pestal et al, 2015; de Reuver et al, 2021; Nakahama et al, 2021). However, unlike ADAR1-null/editing dead models (Wang et al, 2004; Mannion et al, 2014; Liddicoat et al, 2016b), they also reported normalisation of both survival and weaning weight by concurrent loss of LGP2, IFNAR or PKR.

Here, we report generation and analysis of an independent *Adar1*^{P195A} mutant mouse model. Consistent with the published model (Maurano et al, 2021), we find that the P195A allele is well tolerated when heterozygous or homozygous. When the P195A mutation was combined with a p110/p150 null allele, we observed approximately normal weaning weights and long-term survival of ~45% of *Adar1*^{P195A/-} mice. Phenotypic (runted and shortened lifespan) *Adar1*^{P195A/-} animals had evidence of a high ISG signature and a mild tissue type restricted PKR activation and integrated stress response (ISR) signature. The unaffected *Adar1*^{P195A/-} did not show activation of ISGs or the ISR pathway. However, when non-runted *Adar1*^{P195A/-} mice were used for breeding with *Adar1*^{P195A/+}, the next generation of *Adar1*^{P195A/-} were more severely runted with shortened lifespan, however, this was also partially penetrant. The loss of *Ifih1* (MDA5), the primary sensor of unedited cellular dsRNA, prevented activation of the ISG response and rescued the runting, gene expression changes, post-natal lethality, and long-term survival of all genotypes tested. These data do not support the conclusion that the compound P195A mutation leads to fully penetrant integrated stress response pathway activation and shortened lifespan in mice. We further demonstrate that expression of an editing-deficient ADAR1 with P195A (*Adar1*^{P195A/E861A}) prevented the pathology seen in the *Adar1*^{P195A/-} mice in an RNA-editing independent manner.

Results

Generation of an *Adar1* P195A knock-in mutant allele

The P193A mutation in human ADAR1 maps to the Z α domain that is unique to the ADAR1 p150 isoform. The proline 193 residue of human ADAR1 is homologous to murine proline 195 (Fig 1A). We introduced a C-to-G point mutation to generate a proline-to-alanine substitution at amino acid 195 (p.P195A) into murine *Adar1* using CRISPR/Cas9 on a C57BL/6 background (Fig 1B). This resulted in the desired mutation that was confirmed by Sanger sequencing and through restriction digest of genomic PCR products, utilising a silent unique restriction site that was introduced during targeting to the modified locus (Fig 1C). After the identification of heterozygous founder mice (*Adar1*^{P195A/+}), these were bred to C57BL/6 mice to confirm germ-line transmission of the mutant allele (Appendix Fig S1A and B). Second-generation animals were subsequently bred for all experiments.

To assess the expression of the ADAR1p150 protein from the mutant allele, we isolated E13.5 mouse embryonic fibroblasts (MEFs) and treated these with murine interferon beta (IFN β). We tested MEFs from two independent *Adar1*^{+/+} (+/+), *Adar1*^{P195A/+} (P195A/+) and *Adar1*^{P195A/P195A} (P195A/P195A) littermates. Immunoblotting demonstrated that the induction and expression of the p150 isoform following IFN β treatment was intact and equivalent between *Adar1*^{+/+}, *Adar1*^{P195A/+} and *Adar1*^{P195A/P195A} cells (Fig 1D).

ADAR1 P195A mutation alone is well tolerated

The heterozygous *Adar1*^{P195A/+} mice were inter-crossed, and we recovered viable heterozygous and homozygous animals at the expected frequency (Fig 1E), consistent with a previous report

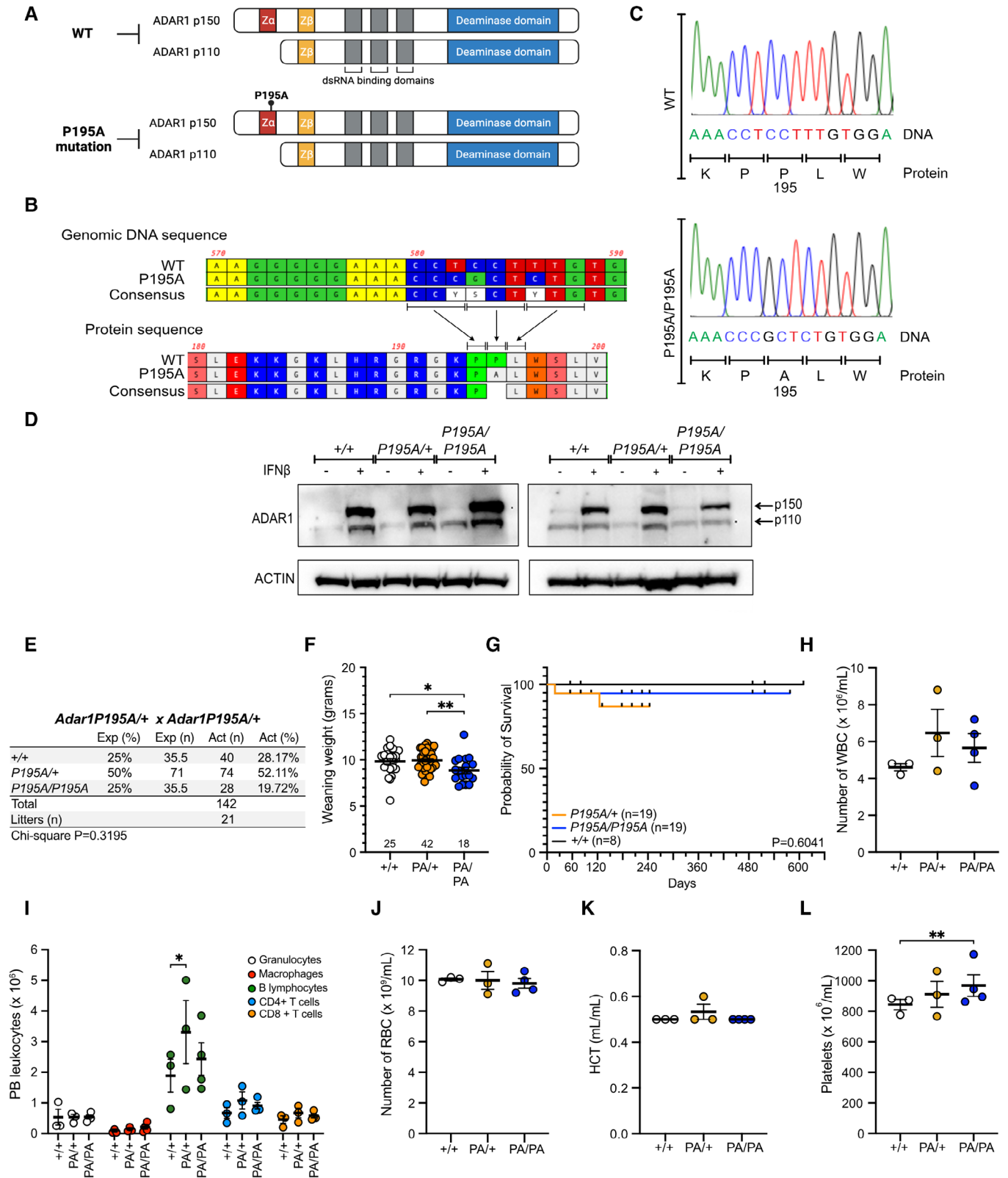


Figure 1.

Figure 1. Generation and characterisation of an *Adar1*^{P195A} knock-in allele.

- A Schematic of the murine wild-type ADAR1 isoforms and the location of the P195A mutation.
 B Genomic alignment and translation of the WT and P195A allele.
 C Sanger sequencing traces and alignments of genomic DNA isolated from animals from *Adar1*^{+/+} (WT) and *Adar1*^{P195A/P195A}.
 D Western blot analysis of ADAR1 expression in E13.5-immortalised MEFs of the indicated genotypes +/- interferon- β (IFN β). Data from two independent cell lines per genotype.
 E Results from inbreeding of *Adar1*^{P195A/+} animals.
 F Weaning weights of mice of the indicated genotypes;
 G Survival analysis of mice of the indicated genotypes; number as indicated for each genotype. Statistical difference determined by Log-rank (Mantel–Cox) test.
 H Total white blood cell counts (WBC) in peripheral blood (PB).
 I Absolute numbers of each lineage in PB. * $P < 0.05$. Significance was determined by a two-way ANOVA test with multiple comparisons.
 J–L Peripheral blood, (J) red blood cell (RBC), (K) haematocrit (HCT) and (L) platelets.

Data information: Data in (F), (H), (J), (K) and (L) represent the mean \pm SEM. * $P < 0.05$; ** $P < 0.01$; Significance determined by ordinary one-way ANOVA with Tukey's multiple-comparison tests (adjusted P -value).
 Source data are available online for this figure.

(Maurano *et al*, 2021). The homozygous *Adar1*^{P195A/P195A} mice had slightly lower weaning weights than the wild-type and heterozygous mice due to a reduction in the weaning weights of the *Adar1*^{P195A/P195A} females (Fig 1F; Appendix Fig S1C). Both *Adar1*^{P195A/+} and *Adar1*^{P195A/P195A} mice have normal lifespans (Fig 1G). Assessment of the peripheral blood cell populations and indices (Fig 1H–K; Appendix Fig S1D and E) demonstrated that the heterozygous and homozygous P195A animals are comparable to wild-type controls. There was a slight but significant elevation of platelet number in the *Adar1*^{P195A/P195A} mutants (Fig 1L) of undetermined significance. Broad-based histopathological analysis demonstrated that the *Adar1*^{P195A/P195A} animals are microscopically normal (Appendix Table S1). Overall, the P195A mutation is not pathogenic in isolation, and mice with this mutation have no apparent disadvantage in normal development and survival.

***In vivo* expression of P195A alone activates an ISG signature but is well tolerated**

To test the acute effects of the P195A mutation in adult mice, we undertook an *in vivo* tamoxifen treatment of *R26-CreER*^{T2} *Adar1*^{fl/+} and *R26-CreER*^{T2} *Adar1*^{fl/P195A} animals (Heraud-Farlow *et al*, 2017). Adult (> 8-week-old) animals were fed a tamoxifen-containing diet for 28 days (Fig 2A). The *Adar1* floxed allele (exon 7–9 floxed) is deleted broadly across the body upon tamoxifen treatment, rendering adult mice expressing only the heterozygous (Δ /+) or only P195A (Δ /P195A) expressing (Fig 2A). Analysis of the genomic DNA derived from bone marrow cells at Day 28 demonstrated efficient and comparable recombination of the *Adar1* floxed allele (Fig 2B; Appendix Fig S2). We did not see evidence for selection against deletion, evidenced by the retention of the floxed allele, as we had previously reported with either the *R26-CreER*^{T2} *Adar1*^{fl/fl} (ADAR1 protein null), *R26-CreER*^{T2} *Adar1*^{fl/p150} (ADAR1p150 null) or *R26-CreER*^{T2} *Adar1*^{fl/E861A} (editing dead ADAR1) in the same experimental model (Heraud-Farlow *et al*, 2017; preprint: Liang *et al*, 2022). In contrast to mice with the loss of the entire protein or impaired editing function that became moribund and required euthanasia prior to 28 days of treatment (Heraud-Farlow *et al*, 2017), both Δ /+ and Δ /P195A animals tolerated the diet well (Fig 2C). There was no significant difference in weight change between the cohorts compared to the weight at Day 0 (Fig 2D).

At day 28 of the tamoxifen diet, we collected peripheral blood (Fig 2E), bone marrow (Fig 2F–H), spleen (Fig 2I and J) and thymus (Fig 2K and L) and assessed haematopoiesis. We found modest changes across these organs in terms of cellularity or lineage distribution/differentiation. The Δ /P195A mice had a lower total number of B lymphocytes in peripheral blood (Fig 2E) and granulocytes in the bone marrow (Fig 2G), neither of which were apparent in the germline *Adar1*^{P195A/P195A} (Fig 1I). We also assessed activation of the ISG response by assessing the expression of Sca-1, an ISG induced in response to a loss of ADAR1 (Essers *et al*, 2009; Hartner *et al*, 2009; Heraud-Farlow *et al*, 2017). There was increased expression of Sca-1 on the cell surface of the Δ /P195A within the lineage negative fraction of the bone marrow (Fig 2M). Prompted by the increased Sca-1 expression, qPCR for the ISGs *Ifit1* and *Irf7* demonstrated a six- to eightfold increased expression of these in the Δ /P195A bone marrow (Fig 2N). We did not find changes in the expression of genes in the integrated stress response (ISR) pathway in the same samples (Fig 2N). The signature of ISR genes was investigated because a previous report utilising the same *Adar1* null allele (*Adar1* exon 7–9 deleted) compounded with the P195A mutation showed an elevated ISR gene expression as the result of PKR activation (Maurano *et al*, 2021). Collectively, these analyses demonstrate that *in vivo* *Adar1* ^{Δ /P195A} animals have a modest acute activation of an innate immune response following somatic restricted expression of P195A. This ISG activation is of a relatively low level compared to the levels seen when animals and cells are engineered to be ADAR1 null, p150 isoform null or editing deficient (Liddicoat *et al*, 2015, 2016b; Heraud-Farlow *et al*, 2017; preprint: Liang *et al*, 2022), and is well tolerated without any effects on the animals' overall well-being or survival. The active ISG signature was also reported in the biochemical $Z\alpha$ mutants indicating that an impaired $Z\alpha$ domain of ADAR1 may induce spontaneous but relatively low IFN response (de Reuver *et al*, 2021; Tang *et al*, 2021), while the mice's overall health and lifespan are unaffected.

ADAR1^{P195A} has a subtle effect on A-to-I RNA editing levels

To understand the effects of this mutation more completely, we undertook RNA-seq of the brain of adult animals (48–74 days of age). The brain was chosen as it is the most affected tissue in AGS patients with ADAR mutation, and we have a detailed understanding in the mouse of the A-to-I RNA editing landscape and ADAR1-

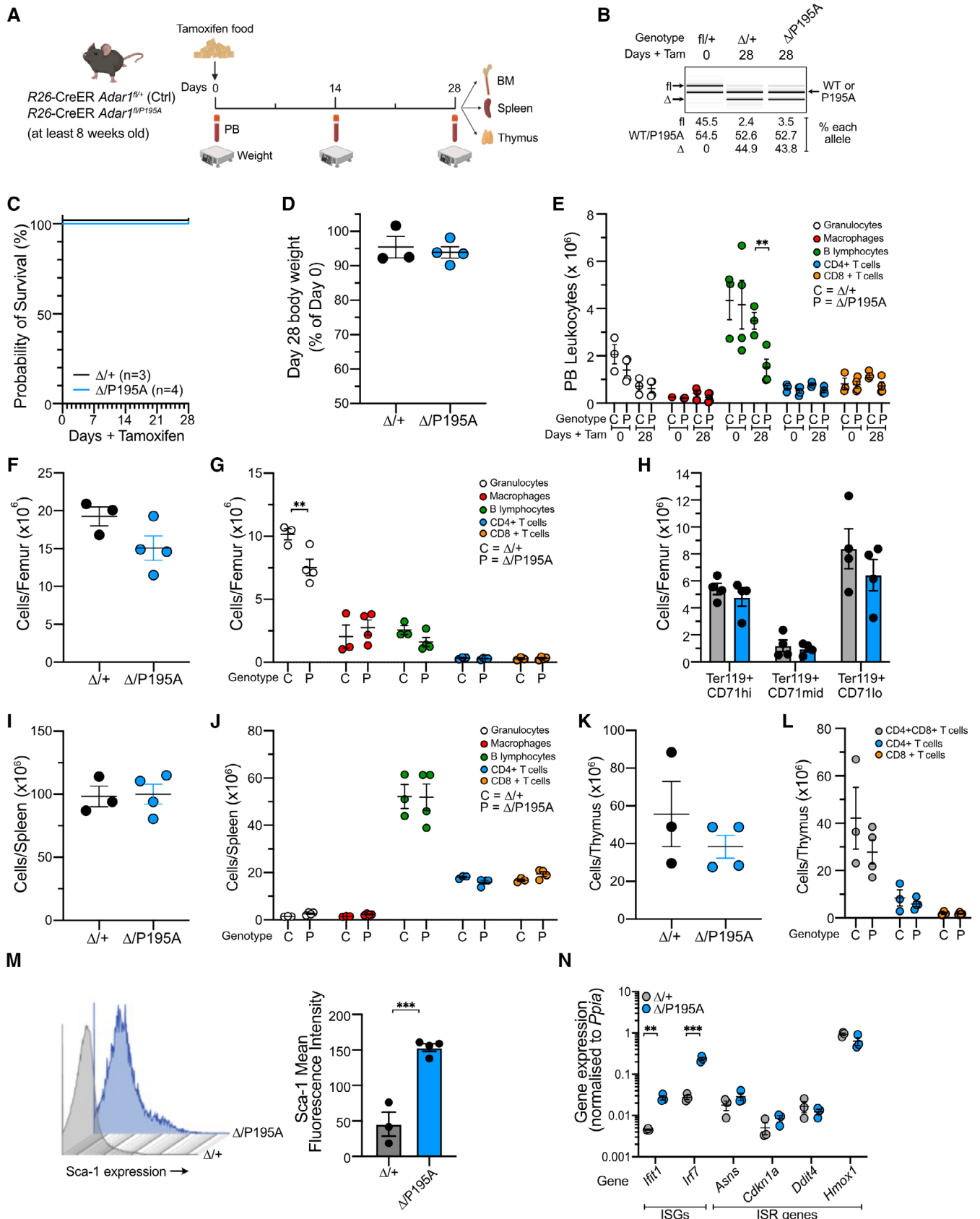


Figure 2.

Figure 2. *In vivo* expression of P195A is well tolerated and results in a modest induction of interferon-regulated gene expression.

- A Schematic outline of the experiment.
 B Representative genotyping of recombination of the *Adar1* floxed allele at day 28 using genomic DNA isolated from whole bone marrow cells. Recombination percentage was calculated using LabChip (PerkinElmer)-based quantitation of band intensity compared to the WT/P195A allele and known standard/marker.
 C Survival analysis of mice of the indicated genotypes; number as indicated for each genotype. No statistical difference between genotypes by Log-rank (Mantel–Cox) test.
 D Percentage change in body weight of each cohort based on comparison of the weight at day 28 of tamoxifen food compared to day 0 (prior to initiation of tamoxifen-containing diet).
 E Peripheral blood leukocyte populations (by lineage) between genotypes at day 0 and day 28.
 F Bone marrow (BM) cellularity.
 G Differential analysis of leukocyte populations in the BM.
 H BM erythroid cells.
 I Splenic cellularity.
 J Differential analysis of leukocyte populations in the spleen.
 K Thymic cellularity.
 L Differential analysis of thymocyte populations in the thymus.
 M Representative flow cytometry histogram of Sca-1 expression between control (*Δ/+*; grey) and P195A only (*Δ/P195A*; blue) expressing BM sample. Quantitation of mean Sca-1 fluorescence intensity within the lineage negative fraction of whole bone marrow.
 N qPCR (SYBR green)-based analysis of indicated gene expression in BM. Data expressed as mean ± SEM gene expression related to *Ppia* expression.

Data information: Unless otherwise stated, data expressed as mean ± SEM; *R26-CreER^{ki/+} Adar1^{fl/+}* (control; *n* = 3) and *R26-CreER^{ki/+} Adar1^{fl/P195A}* (P195A; *n* = 4). All BM, spleen and thymic analysis at day 28 post-tamoxifen treatment; statistical comparison in plots was done by *T*-test (panels D, F, I, K and N) or two-way (panels E, G, H, J, M and L) ANOVA tests with multiple comparisons with statistical significance of *****P* < 0.01** and ******P* < 0.001**.

Source data are available online for this figure.

specific sites within this tissue from previous studies (Chalk *et al*, 2019). We did not find any significantly altered gene expression signatures, and there were only very subtle changes in the overall gene expression programme of the brains of the *Adar1^{P195A/P195A}* compared to *Adar1^{+/+}* controls (Fig 3A). We next assessed the A-to-I editing landscape. We assessed both site-specific editing levels and calculated the editing of repetitive sequences using a murine-modified version of the *Alu* editing index (AEI) (Roth *et al*, 2019). The AEI was not appreciably different when assessed across the genotypes, although this is a global assessment of editing of repetitive sequences and may not reveal subtle changes at a limited number of sites (Fig 3B). Therefore, we assessed the editing levels of individual sites between the *Adar1^{P195A/P195A}* and *Adar1^{+/+}* controls based on previous analysis (Fig 3C; Dataset EV1) (Zhang *et al*, 2014; Heraud-Farlow *et al*, 2017). This demonstrated that most editing was unaffected by the P195A mutation, and only a small fraction (~1.8%) of editing was changed in the *Adar1^{P195A/P195A}* brains (Fig 3D; Appendix Fig S3A–I and S4A–C). Affected sites primarily had increased editing that was likely due to modestly increased expression of *Adar1* transcript, also reported in the biochemical $Z\alpha$ mutant (Fig 3E and F; Dataset EV2; de Reuver *et al*, 2021). We additionally assessed the editing at transcripts known or predicted to be subject to Z-RNA formation, using the list of transcripts identified as bound by Z-RNA antibody, Z22 (Zhang *et al*, 2022). Within this subset of transcripts, only six sites were significantly under-edited (Fig 3G). The overall effect of the P195A mutation on physiological homeostatic editing was subtle and restricted to a small subset of the editing events in the murine brain.

Compound mutants of P195A with an A-to-I editing-deficient *Adar1* allele are normal

In humans, the P195A mutation is most often reported as a compound heterozygous mutation, with the second allele having mutations in or around the deaminase domain or harbouring a variant

likely to result in an *ADAR1* null (Rice *et al*, 2017). To understand the consequences of the P195A mutation compounded with a second mutation, more similar to the mutational spectrum reported in AGS, we crossed the *Adar1^{P195A/+}* mice to an editing-deficient point mutant model (*Adar1^{E861A/+}*) (Liddicoat *et al*, 2015). The E861A mutation renders both p110 and p150 editing deficient (Appendix Fig S1A; Liddicoat *et al*, 2015). *Adar1^{P195A/E861A}* mice were viable and appeared normal (Fig 4A). The *Adar1^{P195A/E861A}*, both males and females, had normal weaning weights compared to control genotypes (Fig 4B; Appendix Fig S5A). Cohorts of mice were allowed to age and monitored for signs of illness or changes in health status. The *Adar1^{P195A/E861A}* animals have survived long-term (> 600 days) with no apparent phenotypes (Fig 4C). To determine if there were any microscopic changes, a histopathological assessment of a cohort of *Adar1^{+/+}*, *Adar1^{P195A/+}* and *Adar1^{P195A/E861A}* at 6–7 months of age was undertaken as we have previously described (Heraud-Farlow *et al*, 2017; Chalk *et al*, 2019). There were no genotype-specific differences or evidence of pathological changes (Appendix Table S1; Dataset EV3). These analyses demonstrate that the P195A mutation is well tolerated, even in the presence of a second allele that has no A-to-I editing activity but does express an ADAR1 protein. This is a distinctive difference between the P195A mutation and the recently reported W197A mutation, where the E861A mutation worsened the post-natal survival of the W197A $Z\alpha$ mutation (Nakahama *et al*, 2021).

Compounding the P195A mutation with an *Adar1* null results in partial penetrant runting and shortened lifespan

In parallel to the editing-deficient mutation, we also crossed the P195A allele to the *Adar1^{+/-}* mice (*Adar1* null allele, exon 2–13 deleted; Hartner *et al*, 2004). In this case, the *Adar1*-null allele does not express any p110 or p150 protein (Appendix Fig S1A), leaving only P195A-mutated ADAR1p150 expressed with WT ADAR1p110 expressed from the same allele. The A-to-I editing levels in the adult

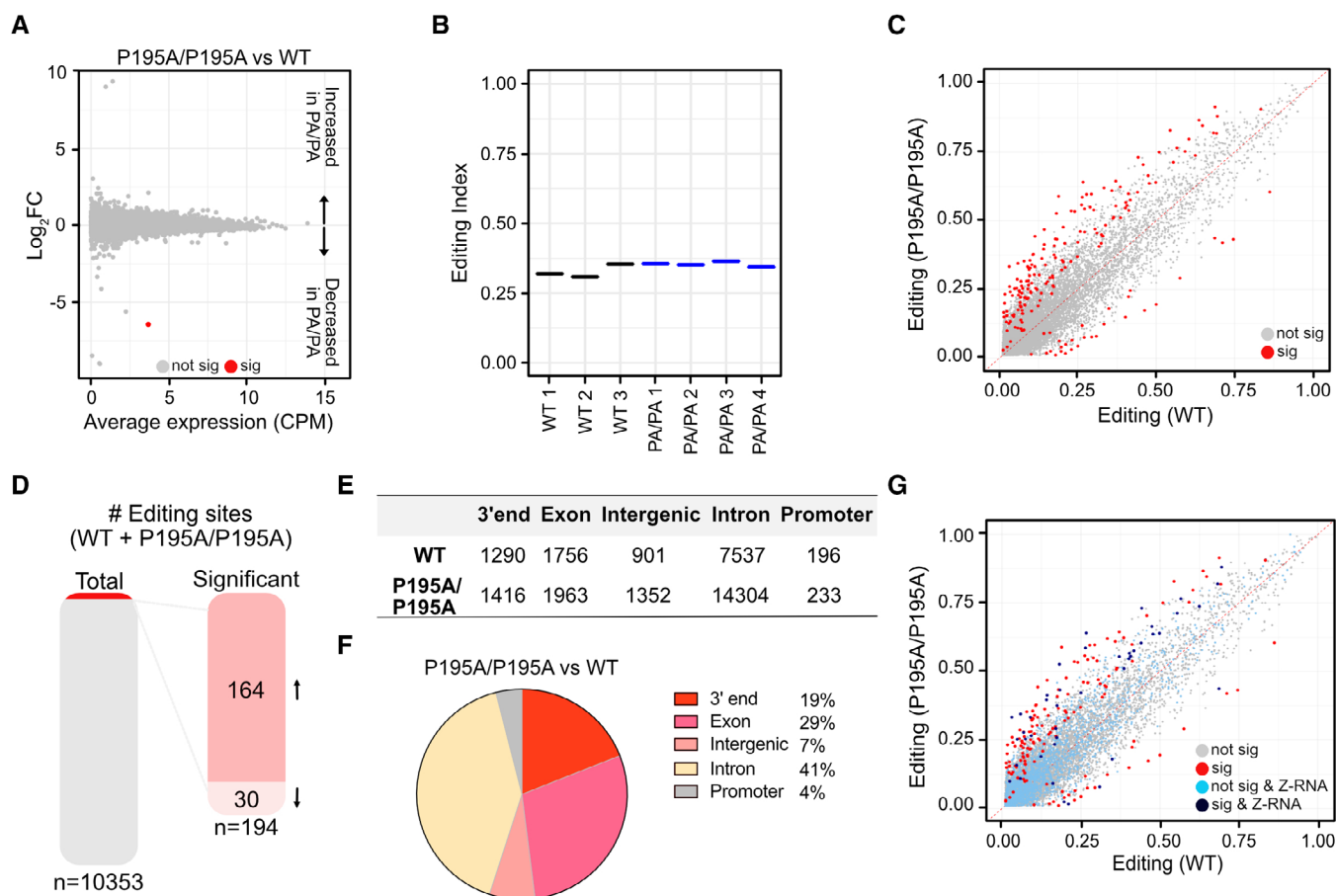


Figure 3. The P195A mutation has a minimal impact on physiological A-to-I editing.

- A** Analysis of differential gene expression from mouse brains of *Adar1*^{P195A/P195A} (P195A/P195A) compared to *Adar1*^{+/+} (WT). Gene expression changes that result in an increased relative gene expression in the *Adar1*^{P195A/P195A} genotype are above the mid-point. Red indicates genes that are significantly different based on abs (log₂FC) > 1, FDR < 0.05.
- B** Murine modified version of the *Alu* editing index (AEI) of all samples of the indicated genotype.
- C** Editing frequency of known sites in P195A/P195A compared to WT by JACUSA. Sites with at least 50 reads and with an editing rate of not < 0.01 (1%). Red indicates the numbers that are significantly different based on the JACUSA call-2 statistic > 5.
- D** Summary of the total A-to-I editing sites shared by both WT and P195A/P195A mice and the number of up-edited or down-edited sites in P195A/P195A compared to WT.
- E** Total genomic locations of the edited sites in WT or P195A/P195A.
- F** The genomic distribution of the significant sites in P195A/P195A compared to WT.
- G** Editing frequency of sites and sites in genes reported to be subject to Z-RNA formation in P195A/P195A compared to WT by JACUSA. Light blue indicates sites that pass both editing and the Z-RNA threshold, and dark blue dots represent the significantly differentially edited sites in Z-RNA formation genes.

brain of the *Adar1*^{P195A/-} were comparable to the *Adar1*^{P195A/P195A} (Appendix Fig S3E–H). There was comparable editing of repetitive regions with a small number of individual sites ($n = 12$) significantly differentially edited, only three of which were experimentally defined Z-RNAs (Appendix Fig S4B).

We recovered mice with all possible genotypes (Fig 4D). When considered as a population irrespective of parental genotypes, the *Adar1*^{P195A/-} animals were runted at weaning, albeit with a more variable range of weights, compared to *Adar1*^{+/+}, *Adar1*^{P195A/+} and *Adar1*^{P195A/P195A} (Fig 4D). This cohort of *Adar1*^{P195A/P195A} did not have reduced weaning weight as observed in the *Adar1*^{P195A/+} inbreeding (Fig 1F, Appendix Fig S1C). In the crosses to generate *Adar1*^{P195A/-}, the gender balance favoured male *Adar1*^{P195A/P195A},

and males do not have a reduced weaning weight (Fig 4D; Appendix Fig S6A). The *Adar1*^{P195A/-} mutants had a weaning weight reduction that was due to a significantly reduced weaning weight of females, although a sub-population of runted males was present (Appendix Fig S6A–D). The *Adar1*^{P195A/-} animals had reduced long-term survival with a median of 78 days compared to all other genotypes (Fig 4E). A significant subset of ~45% of the *Adar1*^{P195A/-} animals had normal long-term survival, with the oldest > 480 days of age (Fig 4E). This is consistent with a subset of *Adar1*^{P195A/-} animals that were not runted (Fig 4D).

Since it appeared that there were two distinct groups of *Adar1*^{P195A/-} mice based on both weaning weight (low vs. normal, Fig 4D) and survival (died before 120 days vs. long-term survival,

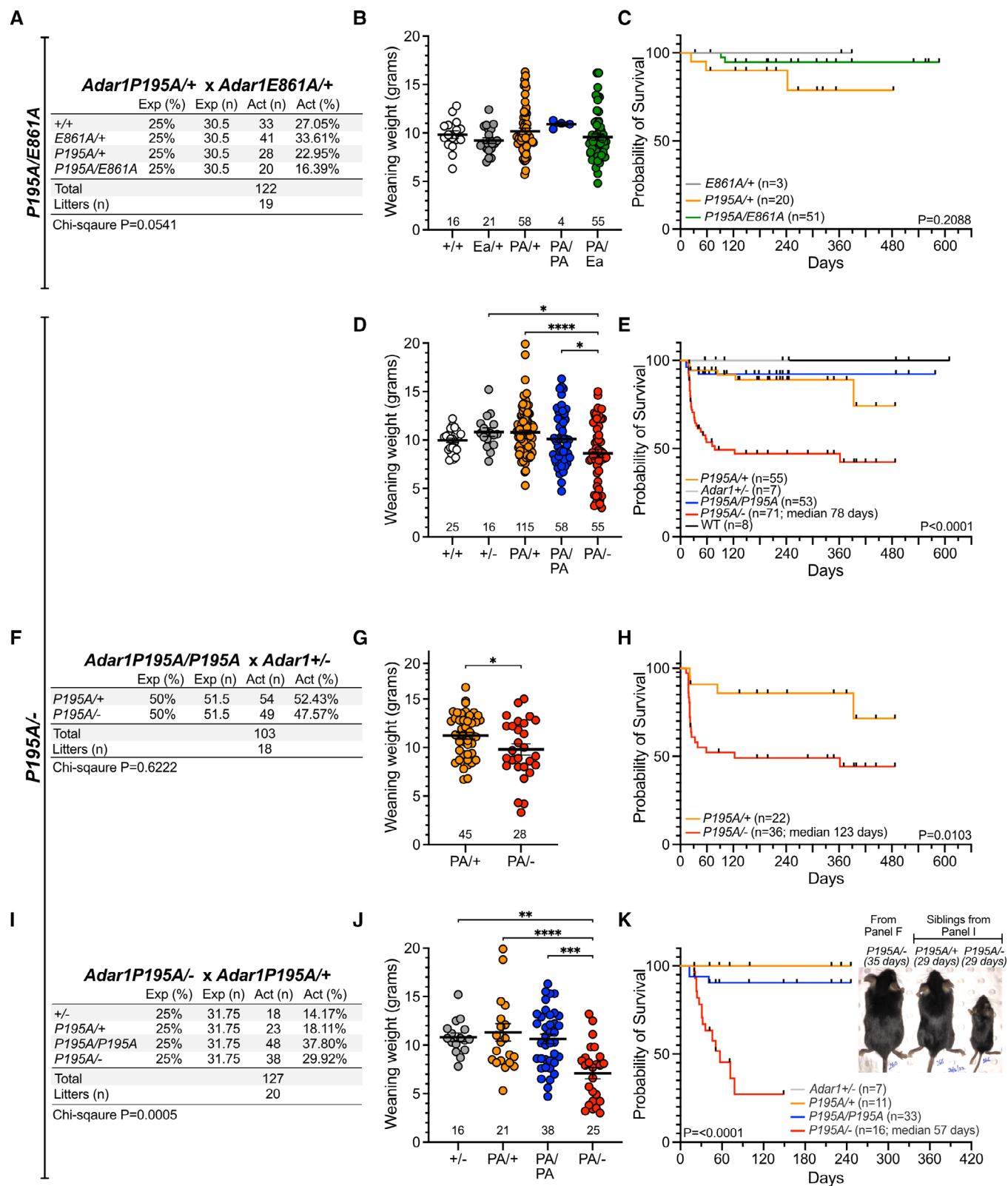


Figure 4.

Figure 4. Weaning weights and survival of *Adar1*^{P195A/E861A} and *Adar1*^{P195A/-} animals.

A–C (A) Results from inbreeding of *Adar1*^{P195A/E861A} animals, (B) weaning weights and (C) survival analysis of mice of the indicated genotypes.
 D, E (D) Weaning weights and (E) survival of mice from inbreeding to generate *P195A*^{-/-} animals.
 F–H (F) Results from breeding of *Adar1*^{P195A/P195A} animals with *Adar1*^{+/-} animals, (G) weaning weights and (H) survival of pups derived from breeding of an *Adar1*^{P195A}^{P195A} to an *Adar1*^{+/-} animal; number as indicated for each genotype.
 I–K (I) Results from breeding of *Adar1*^{P195A/-} animals with *Adar1*^{P195A/+} animals, (J) weaning weights and (K) survival of pups derived from breeding an *Adar1*^{P195A/-} to an *Adar1*^{P195A/+} genotype; number indicated for each genotype. Inset photo: 35-day-old *Adar1*^{P195A/-} male bred from *Adar1*^{P195A/P195A} × *Adar1*^{+/-} parents (data in Panel F); and sibling 29-day-old *Adar1*^{P195A/+} and *Adar1*^{P195A/-} male bred from an *Adar1*^{P195A/-} × *Adar1*^{P195A/+} (data in Panel I).

Data information: The significance of the frequency of genotype (A, F and I) was performed by Chi-square test and weaning weights in (B), (D) and (J) by ordinary one-way ANOVA with Tukey's multiple-comparison test (adjusted *P*-value). Statistical analysis of weights in panel G used an unpaired *t*-test (two-sided). Significance difference in survival plots used Log-rank (Mantel–Cox) test. Weaning weights are presented as mean ± SEM. **P* < 0.05; ***P* < 0.01; ****P* < 0.001; *****P* < 0.0001.

Fig 4E), we further assessed the outcomes based on the breeding pair genotypes. We noted a difference in survival and weaning weights of pups bred from pairs of *Adar1*^{P195A/P195A} × *Adar1*^{+/-} (Fig 4F–H) compared to *Adar1*^{P195A/-} × *Adar1*^{P195A/+} (Fig 4I–K). *Adar1*^{P195A/-} offspring from the *Adar1*^{P195A/P195A} × *Adar1*^{+/-} cross (Fig 4F), had a modestly reduced weaning weight compared to their *Adar1*^{P195A/+} controls (Fig 4G; Appendix Table S2) and a median survival of 123 days (Fig 4H). There was ~ 55% mortality in the first 2 months of life but, after this, the *Adar1*^{P195A/-} survived long-term. As with previous crosses, a reduced weight of the female *Adar1*^{P195A/-} pups contributed to the lower overall weaning weight (Appendix Fig S6). When the adult *Adar1*^{P195A/-} mice were used for breeding, the *Adar1*^{P195A/-} offspring from these parents had more significantly reduced weaning weights and ~ 70% lethality by 80 days of age (Fig 4I–K). In this instance, both male and female *Adar1*^{P195A/-} pups had reduced weaning weights while littermates of other genotypes had a normal weaning weight and survival (Appendix Fig S6C and D, Table S2). The difference in weaning weight based on the parental genotype was not observed in the *Adar1*^{P195A/E861A} animals (Appendix Fig S5B–D, Table S2). These results suggested that a contributor to the phenotype of the *Adar1*^{P195A/-} animals was the genotype of the parent, with an *Adar1*^{P195A/-} parent more often resulting in runting and poor survival specifically of *Adar1*^{P195A/-} pups (Appendix Fig S6C and D). The *Adar1*^{P195A/-} genotype more closely approximates that of an AGS patient, and we cannot find literature to indicate if humans with similar genotypes can successfully rear children. We next investigated whether the maternal or paternal genotype determined the offspring's phenotype. Three *Adar1*^{P195A/-} females and three *Adar1*^{P195A/-} males have been used for breeding in this study. We found that the death of *Adar1*^{P195A/-} pups occurred stochastically and that there was no clear association between the outcomes and the *Adar1*^{P195A/-} parents' gender (Appendix Fig S7A). Similar observations were seen in pups from the *Adar1*^{P195A/P195A} × *Adar1*^{+/-} breeding pairs (Appendix Fig S7B). The *Adar1*^{+/-}, *Adar1*^{P195A/+} or *Adar1*^{P195A/P195A} littermates from these same breeding pairs had no runting indicating that post-natal maternal care was not a clear contributor to the phenotype (Fig 4I–K).

We undertook an assessment of the normal and runted *Adar1*^{P195A/-} animals to understand how and why they were presenting with distinctive phenotypes despite the same genotype and environmental conditions (housing, food, bedding, etc.). Histopathology analysis did not identify any genotype-specific defects in the control C57BL/6, *Adar1*^{P195A/+}, *Adar1*^{P195A/P195A}, *Adar1*^{P195A/E861A} mice or in the normal size *Adar1*^{P195A/-} animals in the brain,

liver, kidney and spleen (Appendix Table S1; Dataset EV3–EV5). In contrast, the runted *Adar1*^{P195A/-} mice (aged from 29 to 62 days) had multiple pathological abnormalities (Appendix Table S1; Dataset EV5). Of four mice assessed, one mouse had evidence of inflammation in the brain, and three mice had pathologies in the liver and kidney. As previous studies demonstrated physiological functions for ADAR1 and for the Zα domain of p150 in regulating murine haematopoiesis (Hartner et al, 2009; Liddicoat et al, 2015; Nakahama et al, 2021), we collected peripheral blood, bone marrow, spleen and thymus for analysis. In the peripheral blood, almost all parameters and cell populations were significantly reduced in the runted *Adar1*^{P195A/-} mice, whereas the non-runted *Adar1*^{P195A/-} had populations comparable to the heterozygote *Adar1*^{P195A/+} and homozygous *Adar1*^{P195A/P195A} mice (Appendix Fig S8A–L). Similar reductions were seen across the bone marrow, spleen and thymus (Appendix Fig S9A–S). The reduction in the haematopoietic cell populations in the runted *Adar1*^{P195A/-} animals indicated a requirement of ADAR1 protein, and potentially its interaction with Z-RNA, for normal haematopoiesis. These abnormalities were absent in the normal-size *Adar1*^{P195A/-} mice that survive long term, suggesting additional contributors to the development of these phenotypes are not entirely genotype dependent. Collectively, our results demonstrate that expression of an ADAR1 protein, even if editing deficient, is essential to prevent pathology development in an RNA-editing independent manner. However, the incomplete phenotypic presentation of the *Adar1*^{P195A/-} animals could be partly attributed to the parental genotypes, but importantly, other non-genetic factors contribute that remain to be elucidated. Interestingly, these observations are reminiscent of humans with P193A mutation-related diseases, where there is variable age and severity of disease onset (Rice et al, 2017).

Loss of MDA5 prevents runting and premature lethality of *Adar1*^{P195A/-} animals

Based on the established role of MDA5 (gene *Ifih1*) in sensing and responding to unedited cellular dsRNA (Liddicoat et al, 2015), we generated *Adar1*^{P195A/E861A}*Ifih1*^{-/-} animals from different breeding combinations (Fig 5A and B; Appendix Fig S5E–I). *Adar1*^{P195A/E861A}*Ifih1*^{-/-} animals were comparable to control littermates and had a normal weaning weight and long-term survival. Next, we sought to determine if loss of MDA5 would prevent the runting and post-natal lethality of the *Adar1*^{P195A/-} in the first 100 days of life. We generated cohorts of animals on both an *Ifih1*^{+/-} and *Ifih1*^{-/-} background. Homozygous deletion of MDA5 completely normalised

the weaning weights and prevented the premature death we had observed in a subset of *Adar1*^{P195A/-} animals with no statistical difference in survival across all genotypes assessed (Fig 5C and D; Appendix Fig S10A–G; Table S2). The *Adar1*^{P195A/-} *Ifih1*^{-/-} mice were generated (Appendix Fig S10A and D). *Adar1*^{P195A/-} *Ifih1*^{-/-} animals derived from *Adar1*^{P195A/-} *Ifih1*^{-/-} × *Adar1*^{P195A/+} *Ifih1*^{-/-} (or *Adar1*^{P195A/P195A} *Ifih1*^{-/-}) breeding pairs were rescued by MDA5 deletion (Appendix Fig S10A–F). Therefore, MDA5 is the primary physiological sensor of unedited cellular RNA that mediates the pathology and phenotypes we observed in the subset of *Adar1*^{P195A/-} animals. Interestingly, heterozygosity for MDA5 also rescued weaning weights and extended survival of the *Adar1*^{P195A/-} mice (Appendix Fig S11A and B). The *Adar1*^{P195A/-} *Ifih1*^{+/-} and *Adar1*^{P195A/-} *Ifih1*^{-/-} weights were not significantly different. Histopathology analysis demonstrated that the abnormalities observed in the runted *Adar1*^{P195A/-} mice were largely absent in *Adar1*^{P195A/-} *Ifih1*^{-/-} mice, with two of the three *Adar1*^{P195A/-} *Ifih1*^{-/-} mice having kidney pathology, indicating a potential MDA5 independent change (Appendix Table S1; Dataset EV4). These analyses demonstrated that loss of MDA5 alone was sufficient to restore viability and long-term survival of the *Adar1*^{P195A/-} animals.

Runted *Adar1*^{P195A/-} mutants have an elevated ISG expression and tissue-specific ISR activation

Analysis of ADAR1p150 α mutations had reported activation of the interferon-stimulated gene programme and, in the case of the previously reported P195A mutant, activation of the PKR-related integrated stress response (Maurano et al, 2021; Nakahama et al, 2021). We assessed the ISG and ISR signatures in the RNA-seq datasets we had generated (Liu et al, 2019; Wong et al, 2019). When we compared the ISG signature between *Adar1*^{+/+}, *Adar1*^{P195A/P195A} and *Adar1*^{P195A/-} (non-runted) animals, there was no significant induction of ISGs in the *Adar1*^{P195A/-} samples (Fig 6A top panels), or activation of the ISR signature (Fig 6A lower panels, Appendix Fig S12A). To determine if other α mutations impacted these pathways, we assessed the brain RNA-seq datasets from the W197A mutant mice (Nakahama et al, 2021), and a recently reported RNA-seq dataset from spleens of the previously reported *Adar1*^{P195A/p150-}, which included a PKR-deficient cohort (*Eif2ak2*^{-/-}) (Hubbard et al, 2022). The *Adar1*^{W197A/W197A} mutants display a fully penetrant runting and the majority die by 40 days of age (Nakahama et al, 2021), a more severe phenotype than that observed with the P195A mutants we generated. The available dataset was from whole brain so was more directly comparable to the RNA-seq datasets we generated. Analysis of the brain transcriptome demonstrated that the W197A homozygous mutants had an active ISG signature, but no significant activation of the ISR gene set compared to their *Adar1*^{+/+} control samples (Fig 6B, Appendix Fig S12B). The analysis of the previous P195A model had concluded that PKR activation and the subsequent integrated stress response were responsible for the immunopathology of the P195A mice (Maurano et al, 2021). We initially accessed the dataset from Maurano et al (NCBI GEO: GSE162583) but it was very limited in depth (5 million read targets) and at 58 bp single-end reads which restricted analysis. The same group more recently reported a second RNA-seq dataset from the spleen of 23-day-old mice, and we assessed both the ISG and ISR transcriptional response in these samples (Hubbard et al, 2022).

Importantly, in the newer dataset, there were WT, *Adar1*^{P195A/p150-} and an *Adar1*^{P195A/p150-} *Eif2ak2*^{-/-} (PKR null) cohort, allowing a direct assessment of PKR and the ISR (Hubbard et al, 2022). In these samples, there was evidence of activation of the interferon-stimulated gene signature in both the *Adar1*^{P195A/p150-} and *Adar1*^{P195A/p150-} *Eif2ak2*^{-/-} (PKR null), albeit with a high level of variability between individuals of the same genotype (Fig 6C, Appendix Fig S12C). There was no significant enrichment of the integrated stress response gene set by QuSAGE analysis (Fig 6C; Appendix Fig S12C). The direct comparison of the PKR-sufficient (*Adar1*^{P195A/p150-}) and -deficient (*Adar1*^{P195A/p150-} *Eif2ak2*^{-/-}) datasets enabled a conclusion that there is limited evidence in the transcriptome data that defines a PKR-dependent gene signature, even though it was shown genetically to be consequential (Maurano et al, 2021).

To broaden our assessment, we isolated RNA from brain, liver and kidney tissues from C57BL/6 mice (WT; *n* = 3), *Adar1*^{P195A/+} (*n* = 9), *Adar1*^{P195A/P195A} (*n* = 4), *Adar1*^{P195A/E861A} (*n* = 5), normal-size *Adar1*^{P195A/-} (*n* = 7), runted *Adar1*^{P195A/-} (*n* = 5), *Adar1*^{P195A + -} *Ifih1*^{-/-} (*n* = 3) and *Adar1*^{P195A/-} *Ifih1*^{-/-} (*n* = 3). We used the same Taqman-based qPCR assays as described in the original P195A mouse model description (Maurano et al, 2021) to assess the expression of the ISGs *Oas1a*, *Ifi27* and *Irf7* (Fig 6D–F; top panels), and ISRs *Asns*, *Cdkn1a* and *Hmox1* (Fig 6D–F; lower panels). In the brain (Fig 6D) and liver (Fig 6E) but not the kidney (Fig 6F), the *Adar1*^{P195A/E861A} mice had mildly elevated expression of one ISG (*Oas1a*) with variability in the level of increased expression between individuals and tissues. ISG expression in the WT, *Adar1*^{P195A/+} and *Adar1*^{P195A/P195A} mice was not altered in all three organs. While the ISG signature was absent in the *Adar1*^{P195A/-} that had normal body weights, the runted *Adar1*^{P195A/-} animals had a significantly elevated ISG level (*Oas1a* and *Ifi27*). The activated ISG signature is consistent with that reported by Maurano et al (2021) and in other α -domain mutants (de Reuver et al, 2021; Nakahama et al, 2021; Tang et al, 2021). The ISG induction in the runted *Adar1*^{P195A/-} mice was more significant than in the *Adar1*^{P195A/E861A} animals, suggesting that the presence of the editing-deficient ADAR1 protein was modifying the *in vivo* response (Fig 6D–F; top panels). The induction of the ISGs was completely prevented by the deletion of MDA5, as seen in the *Adar1*^{P195A/-} *Ifih1*^{-/-} samples (Fig 6D–F; top panels), consistent with the known function of MDA5 as the primary physiological sensor of unedited cellular dsRNA (Mannion et al, 2014; Liddicoat et al, 2015; Pestal et al, 2015).

Based on the proposed activation of the ISR in the previously reported P195A model (Maurano et al, 2021), we assessed the expression of *Asns*, *Cdkn1a* and *Hmox1* (Fig 6D–F, lower panels). We saw an increase in *Asns* and *Cdkn1a* expression in the runted *Adar1*^{P195A/-} mice with large variations between individuals and tissue types, similar to that reported (Maurano et al, 2021). In our animals, the ISR gene signature was highest in the kidney and to some extent the liver but absent in the brain. Prompted by the more consistent result from kidney, we performed immunoblotting of kidney samples from the same cohort of mice used for qPCR. These demonstrated elevated levels of phosphorylated eIF2 α , a substrate of PKR used in murine samples as a surrogate for PKR activation due to the lack of an antibody for phosphorylated PKR in mouse (Fig 6G). We further assessed p-eIF2 α levels in the thymus, a tissue that has high ADAR1p150 isoform expression (Kim et al, 2021). The thymus of the runted *Adar1*^{P195A/-} mice had increased MDA5 expression, itself

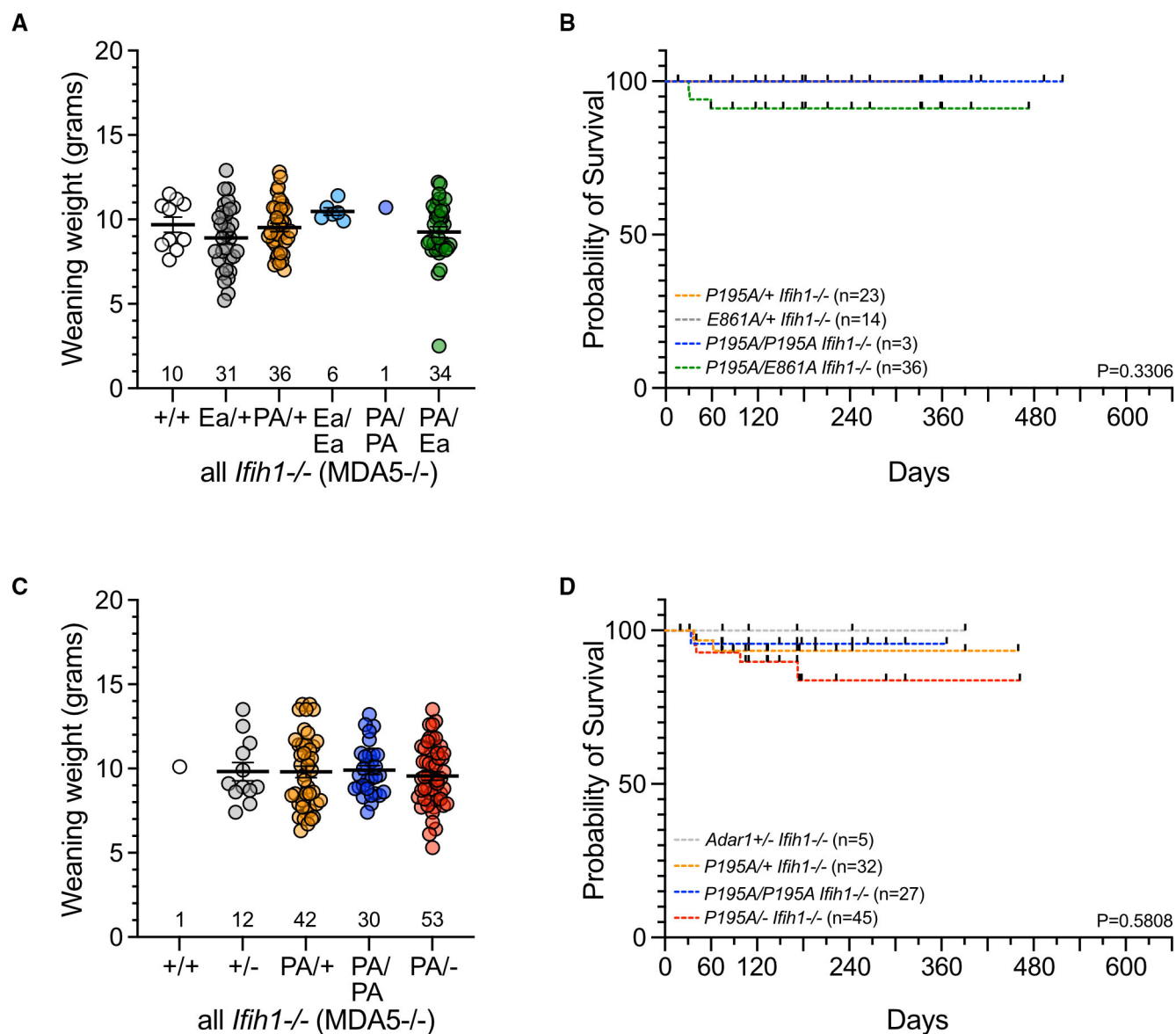


Figure 5. Loss of MDA5 rescues both the weight and viability of *Adar1*^{P195A/-}.

A, B (A) Weaning weights and (B) survival of *Adar1*^{P195A/E861A}*Ifih1*^{-/-} and littermates (all *Ifih1*^{-/-}).

C, D (C) Weaning weights and (D) survival of *Adar1*^{P195A}*Ifih1*^{-/-} and littermates (all *Ifih1*^{-/-}).

Data information: Weaning weights are presented as mean ± SEM. No statistically significant difference across any comparison (ordinary one-way ANOVA with Tukey's multiple-comparison test) in (A) and (C). No statistical difference between genotypes by Log-rank (Mantel-Cox) test in (B) and (D).

an ISG, but there was no increased p-eIF2 α (Appendix Fig S12D). Collectively these analyses indicate a complex and variable phenotype in the *Adar1*^{P195A/-} animals. Those that have a normal size do not show evidence of either ISG or ISR activation. The runted and moribund *Adar1*^{P195A/-} animals show evidence of an MDA5-dependent ISG response. There is also some evidence of PKR and ISR activation, however, this is variable within the runted cohorts and shows differences between tissues even within the same animals. Importantly, the PKR and ISR activation is dependent on MDA5 activation, as MDA5 loss prevented activation in the *Adar1*^{P195A/-} animals.

Adar1^{P195A/-} cells are sensitised to IFN-induced cell death

To assess the cell-intrinsic effect of the P195A mutation, we established HOXA9-immortalised myeloid cell lines (Wang et al, 2006) using bone marrow from adult (> 8-week-old) *R26-CreER*^{T2} *Adar1*^{fl/+} and *R26-CreER*^{T2} *Adar1*^{fl/P195A} animals (Fig 7A). We cultured the cells with and without tamoxifen over a 14-day time course (Fig 7B). As described previously, the *Adar1* floxed is deleted upon tamoxifen treatment, resulting in cells retaining expression of ADAR1 protein (*fl/+* becomes *A/+*) or expressing only the P195A form of ADAR1 (*fl/P195A* becomes *A/P195A*). Notably, these cells

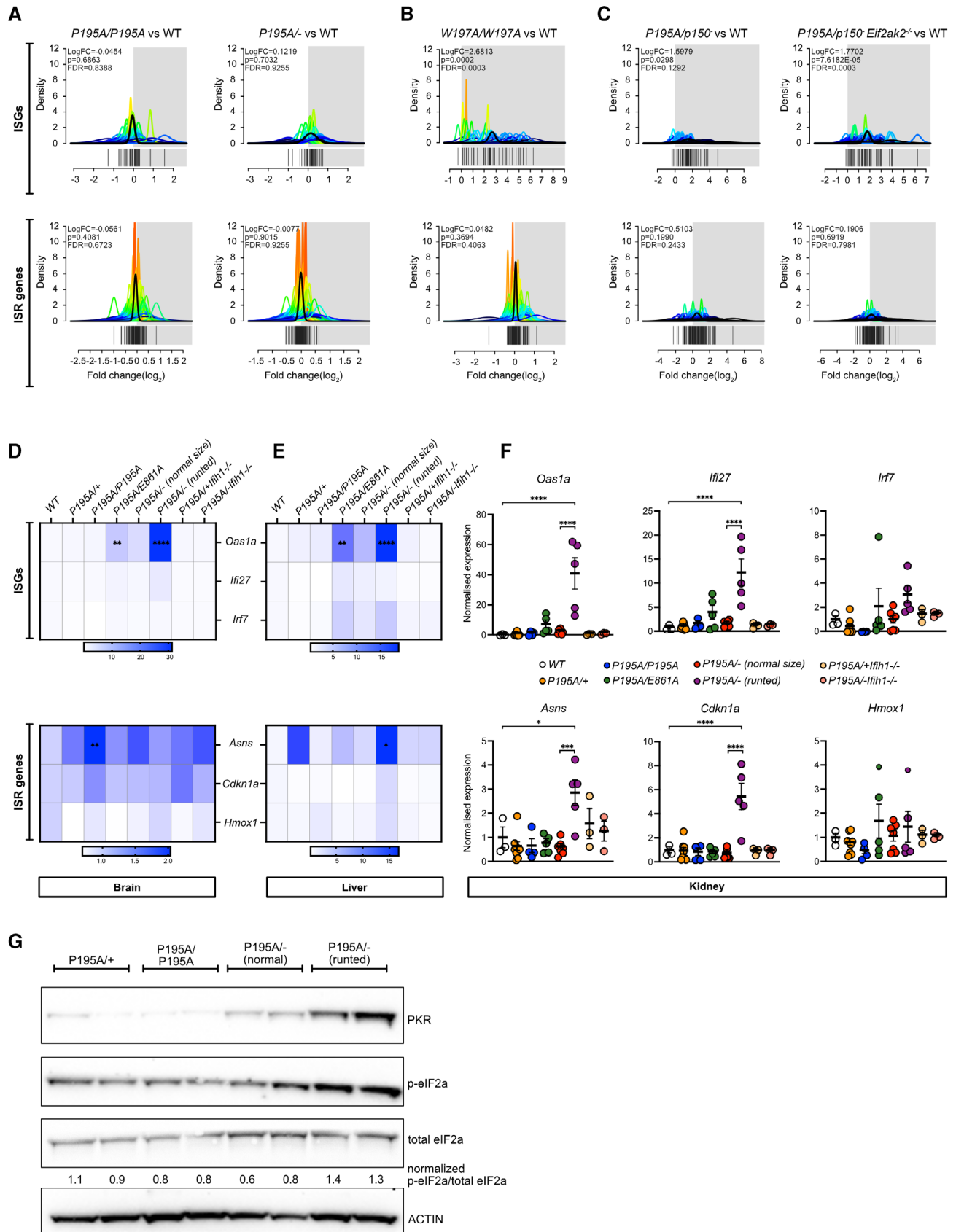


Figure 6.

Figure 6. Upregulation of ISGs and tissue-specific elevation of ISR in *Adar1*^{P195A/-} are MDA5 dependent.

- A QuSAGE analysis using ISGs and ISR gene signatures from previous publications (Material and Methods; Gene set testing (QuSAGE and heatmap analysis)) as the gene set. Every single curve depicts a gene within the barcode. Data from brain samples of *Adar1*^{P195A/P195A} (P195A/P195A) compared to *Adar1*^{+/+} (WT) or *Adar1*^{P195A/-} (P195A/-; non-runted) compared to WT (this study).
- B QuSAGE analysis of ISGs and ISR genes in the whole-brain RNA-seq data of homozygous *Adar1*^{W197A/W197A} compared to WT models published by Nakahama et al, 2021.
- C QuSAGE analysis of ISGs and ISR genes in the spleen RNA-seq data of *Adar1*^{P195A/p150-} or *Adar1*^{P195A/-Eif2ak2^{-/-}} published by Maurano et al (2021).
- D Heatmap representation of the normalised expression of interferon-stimulated genes (*Oas1a*, *Ifi27* and *Irf7*) and the integrated stress response genes (*Asns*, *Cdkn1a* and *Hmox*) in the brain of the indicated genotypes using Taqman-based qPCR.
- E Heatmap representation of the normalised expression of ISGs and ISR genes in the liver of the indicated genotypes using Taqman-based qPCR.
- F Individual plots of the normalised expression of ISGs and ISR genes in the kidney of the indicated genotypes using Taqman-based qPCR.
- G Western blot of PKR, phospho-eIF2 α and total eIF2 α levels in whole kidney lysates derived from the indicated genotypes; same mice as used for panel F. Relative phospho-eIF2 α expression was calculated against total eIF2 α normalised to the average of P195A/+ samples using ImageJ Fiji. All images are from the same gel and re-probed for different antibodies.

Data information: Data presented in panels (D–F) were relative to *Hprt* expression and normalised to the average value of the WT samples. Statistical analysis for all qPCR was two-way ANOVA (D, E) or ordinary one-way ANOVA with multiple-comparison test (F); **P* < 0.05; ****P* < 0.001, *****P* < 0.0001.

Source data are available online for this figure.

employ the same *Adar1* exon 7–9 allele (floxed in our case, whereas germ-line deleted in Maurano et al, 2021) used by Maurano et al (2021). We achieved complete deletion of the *Adar1* floxed allele as assessed by genotyping (Fig 7C; Appendix Fig S13A). The proliferation and viability of three biologically independent P195A cell lines were not affected by treatment with tamoxifen, and the cells behaved in a manner comparable to the control cells (Fig 7D and E). We further assessed if there were changes in ISG expression as cells transitioned to being *Adar1*^{A/P195A}. In contrast to the somatic deletion model (Fig 2) and germ line mutants (Fig 6), we did not see changes in the expression of the ISGs *Ifit1* or *Irf7* by qPCR (Fig 7F). This indicated that in an immortalised myeloid cell, the expression of P195A alone is not sufficient to spontaneously activate an innate immune response to cellular dsRNA. This result suggests that different cell types may respond differently to the P195A mutation, as was reported for a biochemical ADAR1 Z α mutant model (Tang et al, 2021).

We then challenged the *Adar1*^{A/P195A} cells with transfection with high-molecular-weight polyinosinic–polycytidylic acid (polyI:C), a synthetic dsRNA that can activate MDA5, to determine if the P195A mutation altered the response to non-cellular dsRNA. The *Adar1*^{A/P195A} cells did not have a different response to a dose range of polyI:C compared to control cells when assessing the induction of ISGs (Appendix Fig S13B). We additionally treated the cells with either a low or high dose of IFN β . Unexpectedly, and in contrast to the results with polyI:C, IFN treatment resulted in significantly lower cell viability of the *Adar1*^{A/P195A} cell lines as the IFN concentration increased (Fig 7G). Despite the increased cell death, there was a comparable level of ISG induction as assessed by qPCR for *Ifit1* and *Irf7* (Fig 7H). Therefore, the P195A, when compounded with a null allele, sensitises to cell death following treatment with Type I interferon.

Discussion

Understanding how disease-associated ADAR1 mutations affect the proteins' function will be critical to the ultimate goal of developing effective treatments for the patients. To this end, the development of preclinical models that mirror human genetics is an important step. The P193A mutation, which specifically impacts the

cytoplasmic ADAR1p150 isoform, is the most reported ADAR mutation in humans with AGS and BSN (Rice et al, 2012, 2017; Livingston et al, 2014). In AGS, the P193A mutation is reported as a compound heterozygous mutation with a second mutation, most often one that either compromises expression of the second allele or is predicted to compromise A-to-I editing by the protein product of the second allele. Intriguingly, the P193A mutation is also present in the general human population. As this is the most common human ADAR1 mutation, it will be important to determine its effect on both ADAR1's canonical function in A-to-I RNA editing and in other protein-dependent functions of ADAR1.

Herein, we describe the independent generation and phenotyping of a murine model of the human P193A mutation. The homologous murine mutation, P195A, is well tolerated and compatible with adult homeostasis when either heterozygous or homozygous. This is consistent with that previously reported using an independently generated P195A knock-in allele by Maurano et al (2021). While homozygosity for P193A is a rare occurrence in the general human population (Karczewski et al, 2020) and has not been reported in AGS patients (Rice et al, 2012, 2017), all groups have established viable and ostensibly normal *Adar1*^{P195A/P195A} mice. The present data demonstrate that this mutation is well tolerated and does not significantly compromise ADAR1p150's physiological functions *in vivo* under normal laboratory conditions. Detailed analysis of the effects of P195A on A-to-I editing demonstrated that there are very subtle changes, with < 2% of editing sites having differential editing. The limited effect of P195A on editing is consistent with the analysis of editing reported from other murine Z α alleles and from analysis of editing by ADAR1p150 in human cells (de Reuver et al, 2021; Nakahama et al, 2021; preprint: Sun et al, 2022). Direct comparisons of the editing changes between the P195A mutant and the biochemical Z α mutant are confounded by the different tissues (for P195A mutants here, whole adult brain was assessed; and for Z α mutants, P1 brain, spleen and lung or FACS, sorted lung endothelial cells) and age of animals used in each respective study (de Reuver et al, 2021; Jiao et al, 2022). It may also reflect a potentially limited number of physiologically formed Z-RNAs in contrast to Z-RNA levels when animals/cells are infected or treated with interferon (Zhang et al, 2022).

The P193A mutation in humans is pathogenic when compounded with a second mutation that either affects expression of the other

allele of *ADAR* or has mutations predicted to impact editing activity of the second allele. We tested this in the P195A mice by crossing to the editing dead, but protein expressing, E861A allele and an *ADAR1* null allele, where both p110 and p150 are deficient (Hartner et al, 2004; Liddicoat et al, 2015). This yielded distinct outcomes.

The *Adar1*^{P195A/E861A} animals were essentially normal, with normal weaning weights and lifespans, albeit with mild ISG activation in some tissues. This demonstrates that A-to-I editing by the non-P195A p150 protein is not essential to suppress the observed phenotypes but is required to prevent MDA5 activation based on ISG

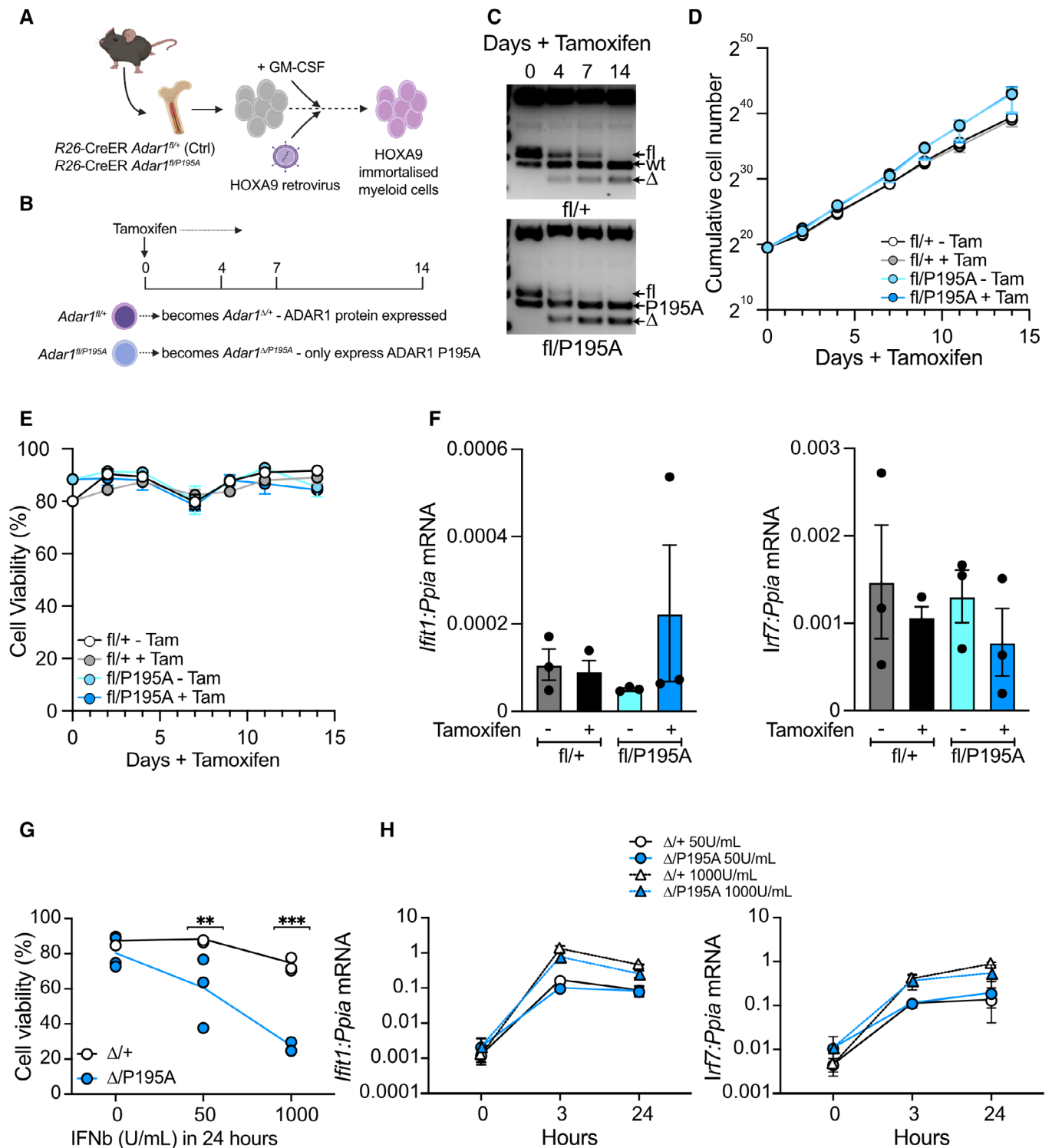


Figure 7.

Figure 7. P195A/I sensitises to cell death following treatment with IFN β .

- A Schematic outline of how the HOXA9-immortalised myeloid cell lines are derived.
 B Experimental outline.
 C Genomic DNA genotyping demonstrating efficient recombination of the floxed *Adar1* allele following tamoxifen treatment.
 D, E (D) Average proliferation and (E) viability of cell lines with and without tamoxifen treatment (isogenic pairs) over 14 days of treatment ($n = 3$ independent lines per genotype; biological replicates).
 F qPCR (SYBR green) analysis of *Ifft1* (left) and *Irf7* (right) expression on day 14 of analysis.
 G Cell viability at IFN β dosages 0, 50 and 1,000 U/ml after 24 h. Statistical analysis was two-way ANOVA with multiple-comparisons correction.
 H qPCR (SYBR green) of *Ifft1* (left) and *Irf7* (right) expression in the cell lines collected at 3 or 24 h post-treatment with 50 or 1,000 U/ml of IFN β . No statistical difference between genotypes in *Ifft1* (left) and *Irf7* (right) expression.

Data information: For data in panels (D) through (H), the experiments were performed with three independently derived cell lines per genotype (biological replicates). The qPCR data are expressed as mean \pm SEM gene expression relative to *Ppia* expression. * $P < 0.05$; *** $P < 0.001$, **** $P < 0.0001$. Source data are available online for this figure.

expression. By comparison, when the E861A allele was compounded with the W197A mutation, the *Adar1*^{W197A/E861A} animals died earlier than the *Adar1*^{W197A/W197A} mice (Nakahama et al, 2021). Proline 195 (193 in humans) is not conserved in the Z α family. It is present in the domain wing and affects the kinetics of binding to left-handed nucleic acids that differ between species (Subramani et al, 2016). Interestingly, mutation of the highly conserved residues involved in binding Z-DNA (N175A/Y179A) (de Reuver et al, 2021; Tang et al, 2021) was well tolerated *in vivo* when homozygous, while the W197A mutant (W195 in human), essential to stabilising the wing, had a fully penetrant *in vivo* phenotype characterised by significant runting and the majority of mice dying by 40 days of age (Nakahama et al, 2021). The comparison of the P195A and W197A results indicates that specific mutations within the Z α domain of ADAR1p150, such as the W197A, reveal specific functions for Z α *in vivo* that warrants further detailed understanding.

A more complex phenotype was presented when the P195A mutation was compounded with an ADAR1 protein-deficient allele (*Adar1*^{P195A/-}), a genotype more closely approximating AGS patients (Rice et al, 2017). In our analysis, the *Adar1*^{P195A/-}, when considered as a population, were modestly runted at weaning but to a lesser extent than that reported by Maurano et al, with an independent P195A allele or by de Reuver et al, with the N175A/Y179A allele that survived < 1 week after birth when compounded with an *Adar1* null allele (de Reuver et al, 2021; Maurano et al, 2021). The mean weaning weights across all genotypes in our study (both as a total cohort or separated by gender; Appendix Table S2) are consistent with the reference data for 3- to 4-week-old animals of C57BL/6 background mice from both the Jackson Labs and the International Mouse Phenotyping Consortium (Dickinson et al, 2016; Appendix Table S3). The wild-type controls reported by Maurano et al (2021) weighed more than 20 g at 23 days of age, indicating that they differed from strains we and others have utilised. Within our colony, ~ 45% of the *Adar1*^{P195A/-} had normal long-term survival, again a distinctive finding from the previously reported P195A allele crossed to the *Adar1*^{4Ex7-9} allele (Maurano et al, 2021). Maurano et al (2021) reported that the majority of their *Adar1*^{P195A/-} mice were significantly runted and die by 30 days of age, with a single animal surviving to 84 days of age. Likewise, *Adar1*^{P195A/p150-} mice, where only the ADAR1p150 allele was deleted on the other allele, were significantly runted and survived only slightly longer (median survival 40 days), with none surviving past 112 days (Maurano et al, 2021). The basis for this profound difference is not immediately apparent

but is important to understand. While differences in vivariums may contribute, it seems unlikely that this is the primary driver of the differences.

We believe that two factors may contribute to the differences. Firstly, we observe differences in both survival and weights of the *Adar1*^{P195A/-} mice based on the breeding pair genotype (Fig 4F–K). When an *Adar1*^{P195A/-} was used for breeding, we see significantly reduced weaning weights and poor survival of both male and female *Adar1*^{P195A/-} pups, but not the other pups in the litters of different genotypes, not dissimilar to that reported by Maurano et al (2021). This is not an absolute finding, as even within the same litters, and therefore, the same maternal and physical environment, there are *Adar1*^{P195A/-} pups with a normal weaning weight and those that are severely runted and die before weaning. It is possible that the runted pups cannot compete with their siblings for milk, exacerbating the runting phenotype. The data indicate not only a contribution from parental genotype but also a stochastic effect that is currently not defined. We speculate that the pups that become runted and have a shortened lifespan encounter a “trigger” that results in elevated ISG expression and activation that they are not able to dampen and resolve. This is supported by the qPCR analysis of ISGs in the runted versus non-runted *Adar1*^{P195A/-} animals, but the precipitating factor has not been defined. One factor may be elevated Type I interferon, as the treatment of *Adar1*^{A/P195A} myeloid cells with Type I IFN demonstrated sensitisation and increased cell death compared to control cells. It is plausible that physiologically, and under homeostatic conditions, there are limited amounts of endogenous Z-RNA formed potentially accounting for the tolerance of being *Adar1*^{P195A/P195A} and partially penetrant phenotype of *Adar1*^{P195A/-}. Type I interferon and specific types of viral infection induce Z-RNA (Zhang et al, 2020, 2022), possibly stimulating the formation of endogenous dsRNA substrates that ADAR1^{P195A} is most compromised in binding. We speculate that higher Type I IFN in some mice yields a more severe phenotype. While poorly understood, the development of symptoms in patients with ADAR mutations who develop AGS is sometimes associated with a recent history of prior vaccination or viral infection, both factors could alter the endogenous immune response and cellular dsRNA load (Rice et al, 2017). When considered alongside the rescue afforded by expression of the E861A allele, the runting and early lethality of *Adar1*^{P195A/-} mice are due to a protein-dependent editing-independent function of ADAR1p150. The rescue by loss of MDA5, however, demonstrates that the initial trigger is most likely an MDA5 ligand.

Another contributor to the differences in the reported P195A phenotypes is the different *Adar1*-deficient alleles used in the respective studies. Maurano *et al* utilised an *Adar1*-deficient allele derived by the germ-line deletion of the conditional *Adar1^{fl}* allele that deletes exon 7 to 9 (Hartner *et al*, 2004, 2009; Pestal *et al*, 2015; Maurano *et al*, 2021). Analysis from Maurano *et al*, and a subsequent study, also utilised an ADAR1p150-specific knockout allele (Maurano *et al*, 2021; Hubbard *et al*, 2022). The consistency between these two alleles suggests a robustness of phenotype, however, both of these alleles have caveats that may be critical in this context. The exon 7–9 allele has recently been demonstrated to yield a truncated, editing-deficient and mislocalised protein product impacting both p110 and p150 isoforms (Bajad *et al*, 2020). The truncated p110 and p150 proteins, while non-functional for A-to-I editing, harbour the potential to interfere with the activity of the P195A p150 protein in the cytoplasm and the wild-type p110 expressed from the P195A allele through substrate competition or dimerisation (Cho *et al*, 2003; Valente & Nishikura, 2007). This could potentially result in a less functional, effectively hypomorphic, P195A p150 and WT p110 when heterozygous. However, we have used this same genotype in both the somatic deletion model (Fig 2) and immortalised myeloid cells (Fig 7), and in both settings, we see tolerance of this genotype. Likewise, based on available data, there is evidence that the p150 null allele used interferes with the IFN-induced expression of ADAR1p110 (Steinman & Wang, 2011; Pestal *et al*, 2015; preprint: Liang *et al*, 2022). This could also create a hypomorphic P195A allele with reduced overall ADAR1 protein. In our study, we have used an exon 2–13 deletion of *Adar1*, demonstrated to be a null allele and not known to express any protein product (Hartner *et al*, 2004). Based on the more severe phenotypes in all $Z\alpha$ mutants when paired with a null allele compared to those homozygous for a $Z\alpha$ mutation (de Reuver *et al*, 2021; Jiao *et al*, 2022), as well as the P195A/E861A reported here, gene dosage contributes to these phenotypes. This is consistent with the difference in survival between *Adar1^{E861A/E861A}Ifih1^{-/-}* and *Adar1^{-/-}Ifih1^{-/-}* mice where protein-dependent editing-independent functions of ADAR1 lead to post-natal lethality of mice (Heraud-Farlow *et al*, 2017). It is possible that the runting and completely penetrant post-natal lethality of the *Adar1^{P195A/-}* mice reported by Maurano *et al* (2021) may be confounded by overall ADAR1 protein levels. When crossed to a true null allele, as we have undertaken, ~45% of *Adar1^{P195A/-}* mice survive to adulthood. It is also important to note that the more disruptive biochemical $Z\alpha$ mutants, not present in humans, caused fully penetrant post-natal lethality when paired with an *Adar1* null allele (another distinct null allele generated from excision of the $Z\alpha$ domain), and rescued by loss of MAVS (de Reuver *et al*, 2021; Jiao *et al*, 2022). There may also be other strain differences such as those immune deficiencies previously reported in some lines of C57BL/6 mice (Koehler *et al*, 2020) or accounting for the high birth weight in the Maurano *et al* study. The ultimate cause of death of the runted *Adar1^{P195A/-}* mice from our cohorts remains to be determined.

The physiologically most important role of A-to-I editing by ADAR1 is to edit cellular/endogenous dsRNA to prevent MDA5-mediated innate immune sensing (Liddicoat *et al*, 2015, 2016a). This has been demonstrated in both mouse models and human cells (Mannion *et al*, 2014; Liddicoat *et al*, 2015; Pestal *et al*, 2015). The P195A mutation is associated with reduced editing of some substrates *in cellulo* (Maurano *et al*, 2021), and we find only a small

percentage of editing sites changed in analysis of whole brain from *Adar1^{P195A/P195A}* animals, including considering RNAs bound by Z22 antibody, categorised as more likely to form Z-RNA (Zhang *et al*, 2022). In both human and mouse, the loss of MDA5-MAVS prevents innate immune activation following the loss of ADAR1 or loss of A-to-I editing by ADAR1. We see rescue of phenotypes of the *Adar1^{P195A/-}* mice by loss of MDA5 with full suppression of ISG expression to baseline levels *in vivo*, consistent with a model where MDA5 is the primary, and initiating, sensor of unedited self-dsRNA. All of the ADAR1 $Z\alpha$ mutants described to date when compounded with a null allele were rescued by loss of either MDA5 (Maurano *et al*, 2021; Nakahama *et al*, 2021) or MAVS (de Reuver *et al*, 2021; Tang *et al*, 2021; Jiao *et al*, 2022). Interestingly, we find a dosage-dependent effect of MDA5 with a degree of genetic rescue afforded by being *Ifih1^{+/-}* (Appendix Fig S11A and B). Collectively, these results demonstrate that the absence of MDA5, and subsequent innate immune response, is sufficient to rescue the effects of ADAR1 P195A $Z\alpha$ mutants.

Previous work has not demonstrated rescue from embryonic lethality of *Adar1^{-/-}* animals by concurrent loss of PKR (*Eif2ak2^{-/-}*) (Wang *et al*, 2004) or by loss of IFNAR (Mannion *et al*, 2014; Liddicoat *et al*, 2016b), unlike the rescue to birth or adulthood by loss of MDA5 (*Ifih1^{-/-}*) or MAVS (*Mavs^{-/-}*) of the *Adar1^{-/-}* or ADAR1 editing-deficient (*Adar1^{E861A/E861A}*) mice respectively (Liddicoat *et al*, 2015; Pestal *et al*, 2015; Heraud-Farlow *et al*, 2017). Based on the ISR signature and genetic crosses, it was proposed that PKR activation was important in the pathology of the P195A mouse models generated by Maurano *et al* (2021), and this was genetically tested and PKR loss rescued the *Adar1^{P195A/ΔEx7-9}* mice. In the tissues of our runted *Adar1^{P195A/-}* animals, there was significantly elevated expression of ISGs and we see some restricted evidence for activation of the PKR-related integrated stress response, however, it is variable across tissues even within the same animal. This is particularly apparent in the RNA-seq analysis. In whole brain transcriptomes, assessed both in our study and the W197A analysis (Nakahama *et al*, 2021), there was no evidence to support a conclusion of an elevated ISR signature. Interestingly, when we reassessed datasets from spleen transcriptomes of the *Adar1^{P195A/ΔEx7-9}* mice (Hubbard *et al*, 2022), the same P195A allele originally reported (Maurano *et al*, 2021), there was no statistically significant enrichment of the gene set defined as representative of the ISR transcriptional response *in vivo*. This dataset included a *Adar1^{P195A/ΔEx7-9}Eif2ak2^{-/-}* (PKR null) cohort, enabling a direct comparison of the role of PKR. There was no consistent indication of a PKR-dependent transcriptional signature. We assessed levels of p-eIF2 α , a marker of PKR activation, in the kidney of the runted *Adar1^{P195A/-}* animals and see an ~50% increase compared to normal sized *Adar1^{P195A/-}* and control animals. It is not clear why only some tissues in the runted *Adar1^{P195A/-}* animals show evidence of activation of PKR, either as p-eIF2 α or transcriptional markers of the ISR response, while the same tissues from a normal-sized *Adar1^{P195A/-}* animals do not. Most recently, it has been proposed that the pathology of the *Adar1^{P195A/-}* animals is due to activation of an alternative protein, ZBP-1 (Hubbard *et al*, 2022). ZBP-1 is the only other mammalian $Z\alpha$ -domain-containing protein and has been linked to aspects of ADAR1 biology (Zhang *et al*, 2022). It is not at present clear how this reconciles with the prior model where activation of PKR and the integrated stress response was proposed as the primary driver of the phenotypes in their *Adar1^{P195A/-}* model (Maurano *et al*, 2021;

Hubbard et al, 2022). Given that knockout of IFNAR also rescued *Adar1^{P195A/p150}* mice, and *Adar1^{P195A/-}* cells in this study are more sensitive to Type I IFN, it may be that PKR and ZBP1 are only activated once IFN signalling is initiated via MDA5/MAVS activation (Zhang et al, 2022). Understanding the pathways and how the different dsRNA sensors are engaged by endogenous dsRNAs will be important to reconcile the genetic rescues of $Z\alpha$ mutants.

In summary, the P195A mutation, homologous to the most common human ADAR1 mutation reported in AGS, is well tolerated *in vivo*. We find a complex, partially penetrant phenotype in the *Adar1^{P195A/-}* mice that is contributed to by both parental genotype and non-genetic (e.g. environmental) factors that we have not yet defined. A significant proportion of the *Adar1^{P195A/-}* mice live normally long term without any apparent pathology. The remainder are runted and have a shortened lifespan. The loss of MDA5 is sufficient to rescue phenotypes seen in the *Adar1^{P195A/-}* mice. These findings are consistent with a role for ADAR1p150 in downregulating the ISG response but do not clearly explain the pathology observed in AGS patients outside of MDA5 being the primary *in vivo* initiator of phenotypes associated with ADAR1 mutations.

Materials and Methods

Ethics statement

All animal experiments conducted for this study were approved by the Animal Ethics Committee of St. Vincent's Hospital, Melbourne, Australia (Protocol number #016/20). Animal studies were conducted in accordance with the Australian code for the care and use of animals for scientific purposes, 8th Edition (2013; ISBN:1864965975). Animals were euthanised by cervical dislocation or CO₂ asphyxiation.

Animals

Adar1^{P195A} mice were generated using CRISPR/Cas9 targeting in C57BL/6 zygotes by the Monash Genome Modification Platform (Monash University, Clayton, Australia). A repair oligo containing a CCT > GCT point mutation resulting in a p.P195A (Proline > Alanine) mutation. The repair oligo also had a silent point mutation (CCT > CCC; Proline > Proline, p.P194P) immediately upstream and a second silent mutation (TTG > CTG; Leucine > Leucine, p.L196L) immediately downstream of the P195A mutation, respectively, that created a *BsrBI* restriction enzyme site and prevented Cas9 from cutting the repaired locus and to be used for genotyping using restriction digest of the genotyping PCR product. Introduction of the mutation was confirmed by Sanger sequencing of the region in both the founders and subsequent generations.

The *Adar^{E861A/+}* (*Adar1^{E861A/+}*; MGI allele: *Adar^{tm1.1Xen}*, MGI: 5805648) (Liddicoat et al, 2015), *Adar^{-/-}* (*Adar1^{-/-}*; exon 2–13 deleted; MGI allele: *Adar^{tm2Phs}*, MGI: 3029862) (Hartner et al, 2004), *Adar^{fl/fl}* (*Adar1^{fl/fl}*; exon 7–9 floxed; MGI allele: *Adar^{tm1.1Phs}*, MGI: 3828307) (Hartner et al, 2004, 2009), *Ifih1^{-/-}* (*Ifih1^{tm1.1Cln}*) (Gitlin et al, 2006) and *Rosa26-CreER^{T2}* (Gt(ROSA)26Sor^{tm1(cre/ERT2)Tyj}) (Ventura et al, 2007) mice have all been previously described and were on a backcrossed C57BL/6 background. All animals were

housed at the BioResources Centre (BRC) at St. Vincent's Hospital. Mice were maintained and bred under specific pathogen-free conditions with food and water provided *ad libitum*. For acute somatic deletion (*R26-CreER^{T2}*), all animals were ≥ 8 weeks of age at tamoxifen initiation; tamoxifen-containing food was prepared at 400 mg/kg tamoxifen citrate (Selleckchem) in standard mouse chow (Specialty Feeds, Western Australia).

Weaning age was determined by animal facility staff independently of investigators based on animal welfare and facility SOPs. Animals are typically weaned at 20–25 days of age. Weaning weights are not available if an animal was found dead before weaning; all animals where genotype was confirmed are included in the survival analysis (where possible, any found dead before weaning were genotyped post-mortem).

Genotyping

Genotyping of the P195A mutants was determined by PCR. The repair oligo carrying the P195A mutation also introduced a silent *BsrBI* immediately upstream of the P195A mutation. The digestion of the genomic DNA PCR product was used to determine the presence of the P195A allele and can discriminate heterozygous and homozygous mutants. The following primers: Primer P1 (5'-ACCATGGAGAGGTGCTGACG-3') and P2 (5'-ACATCTCGGGCCTTGGT GAG-3') were used to obtain a 489 bp product from the wild-type allele, which would yield two fragments (265 and 224 bp products) when digested with *BsrBI* (NEB) for the P195A mutant. The P1 primer was used for Sanger sequencing (Australian Genome Research Facility (AGRF), Melbourne) of the purified PCR product as required. Genotyping of all other lines used was performed as previously described (Liddicoat et al, 2015; Heraud-Farlow et al, 2017).

Histology

Three wild-type (*Adar1^{+/+}*, 2 female (F)/1 male (M)), three *Adar1^{P195A/+}* (2F/1M) and four *Adar1^{P195A/E861A}* (3F/1M) animals at 6–7 months of age were used for histopathology examination as previously described (Heraud-Farlow et al, 2017; Chalk et al, 2019). The wild-type animals were littermate controls of the mutant-bearing animals. Tissue collection and histology were performed by the Phenomics Australia Histopathology and Slide Scanning Service, University of Melbourne. The wild-type animals were identified by the pathologists as "controls," the remaining samples were genotype blinded to the staff and pathologist assessors. The following organs were assessed: adrenal glands, bladder, bone marrow, brain, cecum, cervix, colon, duodenum, epididymes, eyes, gall bladder, harderian glands, head, heart, hind leg (long bone, bone marrow, synovial joint and skeletal muscle), ileum, jejunum, kidney, liver, lungs, mammary tissue, mesenteric lymph node, ovaries, oviducts, pancreas, penis, preputial gland, prostate glands, salivary glands and regional lymph nodes, seminal vesicles, skin, spinal cord, spleen, stomach, tail, testes, thymus, thyroids, trachea, uterus and vagina. The full pathology report and genotypes are available in Dataset EV3.

Additional pathology was performed on the brain, liver, kidney or spleen isolated from wild type (bred and housed in the same facility; $n = 3$), *Adar1^{P195A/+}* ($n = 6$), *Adar1^{P195A/P195A}* ($n = 3$),

normal-size *Adar1*^{P195A/-} ($n = 4$), runtad *Adar1*^{P195A/-} ($n = 4$) and *Adar1*^{P195A/-} *Ifih1*^{-/-} ($n = 3$). Tissue was fixed overnight in 2% paraformaldehyde, transferred to 70% ethanol and then processed, sectioned and stained by the Phenomics Australia Histopathology and Slide Scanning Service, University of Melbourne. The wild-type animals were identified by the pathologists as “controls”; the remaining samples were genotype blinded to the staff and pathologist assessors. The full pathology report and genotypes are available in Datasets EV4 and EV5.

Mouse embryonic fibroblasts

Mouse embryonic fibroblasts (MEFs) were generated from E13.5 embryos of the indicated genotypes. The embryos were dissected, removing the head (used for genotyping), heart and foetal liver and the remaining tissue was used to generate MEFs. The tissue was placed in 1 ml of 0.025% Trypsin–EDTA (Gibco/Thermo Fisher), drawn through an 18G needle/1 ml syringe and then placed at 37°C in a 10 cm² tissue culture plate for 30 min. After 30 min, 10 ml of media (high-glucose DMEM [Sigma], 10% FBS [not heat inactivated, Assay Matrix], 1% Penicillin/Streptomycin [Gibco], 1% Glutamax [Gibco] and 1% amphotericin B [Sigma; 250 µg/ml stock]) was added to the plate and the contents dispersed. The MEFs were incubated in a hypoxia chamber flushed with 5% oxygen/5% carbon dioxide in nitrogen at 37°C. Once the cells were 70% confluent, the cells were trypsinised and passaged onto 10 cm plates in normoxic conditions for all further cultures. MEFs were immortalised with retrovirus encoding an shRNA-targeting murine p53 (*shp53.1224* in LMP vector) (Dickins *et al*, 2005) containing 1% polybrene. The immortalised MEFs of the indicated genotypes were treated with recombinant murine interferon beta (PBL Assay Science; PBL-12405) at 250 U/ml for 24 h in normal growth media. After 24 h, cells were collected by trypsinisation and pellets washed in cold PBS and resuspended in RIPA buffer (20 mM Tris–HCl, pH8.0, 150 mM NaCl, 1 mM EDTA, 1% sodium deoxycholate, 1% Triton X-100 and 0.1% SDS) supplemented with 1× HALT protease inhibitor and 1× PhosSTOP phosphatase inhibitor (Thermo Fisher). Lysates were used for western blotting as described below.

Western blotting

Protein was quantified using the Pierce BCA protein assay kit (Thermo Fisher) on an Enspire multimode plate reader (Perkin Elmer). Lysates from MEFs: indicated genotypes +/- interferon treatment were used and 20 µg of protein extract per sample was loaded. Lysates from kidney and thymus: the whole kidney or thymus cells were homogenised in RIPA buffer containing 1× Halt Phosphatase inhibitor (Thermo Fisher) and 1× Halt Protease inhibitor (Thermo Fisher) and 5 µg (kidney) or 15 µg (thymus) of protein was loaded. All samples were loaded on precast NuPAGE™ 10% or 4–12%, Bis-Tris polyacrylamide gels (Invitrogen) and transferred onto Immobilon-P PVDF membranes (Merck Millipore). Membranes were blocked with 5% milk powder in Tris-buffered saline with Tween (TBST) and incubated at 4°C overnight with rat monoclonal anti-mouse ADAR1 antibody (clone RD4B11; purified from hybridoma supernatant by MATF, Monash University) (Liddicoat *et al*, 2015), rabbit anti-MDA-5 (Cell Signalling, D74E4), rabbit anti-PKR (Abcam, EPR19374), phospho-eIF2α (anti-EIF2S1 [phosphor-S51],

Abcam, ab32157), total eIF2α (Cell Signalling Technology, 5324) and mouse anti-actin (Sigma, A1978). Membranes were then probed with HRP-conjugated goat anti-rat (Thermo Fisher, 31470), anti-rabbit (Thermo Fisher Scientific, 31460) or anti-mouse (Thermo Fisher, 31444) secondary antibodies and visualised using ECL Prime Reagent for chemiluminescent detection on Hyperfilm ECL (Amersham) or iBright FL1500 Imaging system (Thermo Fisher).

Peripheral blood analysis

Peripheral blood (approximately 100 µl) was obtained via retro-orbital bleeding. The blood was red blood cell-depleted using hypotonic lysis buffer (150 mM NH₄Cl, 10 mM KHCO₃ and 0.1 mM Na₂EDTA, pH7.3) and resuspended in 50 µl of FACS buffer for flow cytometry analysis.

Flow cytometry analysis

Prior to flow cytometry, PB, bone marrow, spleen and thymus cells were counted on a Sysmex haematological analyser (Sysmex, Japan). Antibodies against murine B220 (conjugated to APC-eFluor780), CD11b/Mac-1 (PE), Gr1 (PE-Cy7), F4/80 (APC), CD4 (eFluor450), CD8a (PerCP-Cy5.5), Ter119 (PE), CD71 (APC), CD44 (PE-Cy7), Sca-1 (PerCP-Cy5.5), c-Kit (APC-eFluor780), CD150 (PE), CD48 (PE-Cy7), CD34 (eFluor660), CD16/32 (eFluor450) and biotinylated antibodies (CD2, CD3e, CD4, CD5, CD8a, B220, Gr-1 and CD11b/Mac1) were used to quantify cell populations as previously described (Singbrant *et al*, 2011; Smeets *et al*, 2014; Liddicoat *et al*, 2015; Heraud-Farlow *et al*, 2017). Biotinylated antibodies were detected with streptavidin-conjugated Brilliant Violet 605. Antibodies were purchased from eBioscience, BioLegend or BD Pharmingen. Cells were acquired on a BD LSRIIFortessa and analysed with FlowJo software Version 9 or 10.0 (Treestar).

RT-qPCR

Whole bone marrow and myeloid cells +/- tamoxifen treatment were collected, and RNA was isolated using the RNeasy kit with on-column DNase digestion (Qiagen). Mouse tissues were collected (one brain hemisphere, liver and kidney; additional histology was performed on tissue from these same animals) from independent biological replicates. Tissues were collected, immediately snap frozen in liquid nitrogen and stored at -80°C. Frozen tissues were homogenised in Trisure reagent (Bioline) using IKA T10 basic S5 Ultra-turrax Disperser. RNA was extracted using Direct-Zol columns (Zymo Research) as per manufacturer's instruction. cDNA was synthesised using Tetro cDNA synthesis kit (Bioline; used for all cDNA described).

Real-time-PCR was performed using two methods: SYBR green method (for myeloid cell lines and *in vivo* R26-CreER experiments, normalised to *Ppia* as previously described; Heraud-Farlow *et al*, 2017). The sequence of primers used for SYBR green-based qPCR can be found in Appendix Table S4. Alternatively, predesigned Taqman probes for *Oas1a*, *Ifi27*, *Irf7*, *Asns*, *Cdkn1a* and *Hmox1* were used and normalised to *Hprt* (for mouse organs from germline mutant animals). Duplicate reactions per sample were measured using an AriaMx Real-time PCR machine (Agilent) using TaqMan Fast Advanced Master Mix (Applied Biosystems, Thermo

Fisher) and predesigned/inventory FAM-conjugated Taqman primer/probe sets (Applied Biosystems, Thermo Fisher) against murine genes: *Oas1a* (assay ID Mm00836412_m1); *Ifi27* (Mm00835449_g1); *Irf7* (Mm00516788_m1); *Asns* (Mm00803785_m1); *Cdkn1a* (Mm04205640_g1); *Hmox1* (Mm00516005_m1) and control gene *Hprt* (Mm00446968_m1). *Hprt* was used as reference genes for relative quantification using the $\Delta\Delta C_t$ method.

Immortalised myeloid cells

HOXA9 immortalised myeloid cell lines (Wang *et al*, 2006) were established by retroviral infection of Ficoll-depleted bone marrow isolated from three independent adult (> 8-week-old) *R26-CreER^{T2} Adar1^{fl/+}* and *R26-CreER^{T2} Adar1^{fl/P195A}* donor animals. The cells were cultured in IMDM (Sigma) containing 10% FBS (Assay Matrix; non-heat inactivated), 1% Penicillin/Streptomycin (Gibco/Thermo Fisher), 1% Glutamax (Gibco/Thermo Fisher) supplemented with 50 ng/ml recombinant mouse stem cell factor (rmSCF, Peprotech), 10 ng/ml recombinant mouse interleukin 3 (rmIL-3, Peprotech) and 10 ng/ml recombinant human interleukin 6 (rhIL-6, Amgen) for 48 h. After 48 h in culture, 1×10^6 cells were spin infected at 1,100 g for 90 min with ectotrophic packaged HOXA9 retrovirus (HOXA9 plasmid was generously provided by Dr Mark Kamps, University of California San Diego) and 8 μ g/ml hexadimethrine bromide (Polybrene; Sigma). At 48 h post-infection, the cells were passaged into IMDM containing 10% FBS, 1% penicillin/streptomycin and 1% glutamax supplemented with 1% granulocyte-macrophage colony-stimulating factor (GM-CSF)-conditioned medium (from BHK-HM5 cell conditioned medium). Cells were maintained in GM-CSF-containing media after this point. Cell lines were established after 3–4 weeks of culture.

Once stable cell lines were established, they were treated with 200 nM 4-hydroxy tamoxifen (Merck Millipore) to activate CreER recombination which results in cells becoming *A/+* (*fl/+* cells become *Adar1* heterozygous) or *A/P195A* (*fl/P195A* cells only retain expression of P195A after tamoxifen treatment). Cells were counted with Trypan blue using a Countess II automated counter (Thermo Fisher) and then passaged every 2–3 days. Viability and proliferation were assessed by Trypan blue staining and counted using a Countess II and gene expression on cDNA made from cells of the indicated genotypes and assessed by SYBR green-based qPCR as described previously (Heraud-Farlow *et al*, 2017; Chalk *et al*, 2019).

Treatment with pIpC or IFN β : *R26-CreER Adar1^{fl/+}* and *R26-CreER Adar1^{fl/P195A}* cells were treated for 14 days with tamoxifen, genotyped and then *Adar1^{A/+}* and *Adar1^{A/P195A}* cells were transferred to non-tamoxifen supplemented IMDM media for poly(I:C) or interferon beta testing. Three independent cell lines were used per genotype. The cells were treated with a dose range of high-molecular-weight poly(I:C) (1.5–8 kb; 1 mg/ml stock) by nucleofection following the manufacturer's instructions (Lonza 4D-Nucleofector™ Kits). The *Adar1^{A/+}* and *Adar1^{A/P195A}* cells ($n = 3$ /genotype; biologically independent samples) were treated with recombinant murine interferon beta (PBL Assay Science; PBL-12405) at 50 or 1,000 U/ml for 3 or 24 h in normal growth media. RNA was isolated (Qiagen RNA Minikit with on-column DNaseI digest) and cDNA was synthesised as described. Gene expression of

the indicated genotypes was assessed by SYBR green-based qPCR as described previously.

RNA-seq analysis

Samples used for RNA-seq were from whole brain samples of 42- to 74-day-old mice of *Adar1^{+/+}* (2F/1M; $n = 3$); *Adar1^{P195A/+}* (2F/1M; $n = 3$); *Adar1^{P195A/P195A}* (3F/1M; $n = 4$) and *Adar1^{P195A/-}* (2F/1M; $n = 3$; non-runted *Adar1^{P195A/-}* animals). Brain samples were collected, snap-frozen in liquid nitrogen and stored at -80°C . Frozen tissues were homogenised in Trisure reagent (Bioline) using IKA T10 basic S5 Ultra-turrax Disperser. RNA was extracted using Direct-Zol columns (Zymo Research) as per manufacturer's instruction. Each sample contained 2,500 ng RNA and was sent for sequencing in a dry form (Novogene RNA Ambient Tube). cDNA library preparation and 150 bp paired-end sequencing were performed by Novogene (Singapore).

Pre-processing

Sequenced reads (150 bp) were trimmed for adaptor sequence and low-quality reads using fastp (v 0.19.5) (Chen *et al*, 2018). Parameters: --trim_front1 10 --trim_front2 10. Reads mapping to rRNA was removed using Bbmap (parameters: bbsplit.sh minratio = 0.56 minhits = 1 maxindel = 16,000) (Bushnell; BbMap, a short read aligner, <https://sourceforge.net/projects/bbmap/>).

External datasets: RNA-seq from the W197A mutant mouse (DRA011210 and DRA011667; Nakahama *et al*, 2021) was downloaded from DDBJ. Gene counts were determined using Salmon (v1.6.0) versus mm11 gencode vm28. Salmon data were processed using tximeta, and summarised to gene using lengthScaledTPM before formatting for degust (csv). Only Ribo KI and WT brain samples were kept for further analysis. Normalisation and filtering (count > 5, min CPM > 1 in at least three samples) were performed within degust.

Processed kallisto files from Hubbard *et al* (2022) (GSE200854; Hubbard *et al*, 2022), were downloaded and analysed. Data were input using tximport, and summarised to gene level counts before formatting for degust (csv). Normalisation and filtering (count > 2, min CPM > 1 in at least three samples) as well as differential expression were performed within degust.

Editing analysis

Mapping: Trimmed reads were aligned to the MM10/GRCm38 reference genome with transcript annotation (gencode.mm10.vM14.annotation.SEQINS.gtf) with STAR (version 2.6.0c) [PMID: 23104886] using the following parameters: --outFilterType BySJout --outSAMattributes NH HI AS NM MD --outFilterMultimapNmax 20 --outFilterMismatchNmax 999 --outFilterMismatchNoverReadLmax 0.04 --alignIntronMin 20 --alignIntronMax 1000000 --alignMatesGapMax 1000000 --alignSJoverhangMin 8 --alignSJDBoverhangMin 1 --sjdbScore 1 --sjdbOverhang 149. Duplicate reads were marked with Picard ["Picard Toolkit." 2019. Broad Institute, GitHub Repository. <http://broadinstitute.github.io/picard/>; Broad Institute].

Known sites: A database of 135,697 murine editing sites was compiled from published databases (RADAR; Ramaswami & Li, 2014), publications (Liddicoat *et al*, 2015; Heraud-Farlow *et al*,

2017; Chalk *et al*, 2019) and unpublished murine datasets (JH-F, AMC and CRW) and the datasets assessed for editing at these sites. Sites were marked as hyper-edited if there were > 10 editing sites within 100 bp, no consideration was made about editing level or if editing occurred in this dataset. See Dataset EV1.

Calling known sites: Editing calling of known sites (RNA vs. mm10) was performed using JACUSA 2.0.0-RC5 (Piechotta *et al*, 2017) (<https://github.com/dieterich-lab/JACUSA>): parameters used: -F 1024 -filterNH_99, -filterNM_99 and -c 3 -P RF-FIRSTSTRAND. Briefly, call-1 was used to determine the RNA editing level for all known sites for each individual sample replicate. Duplicate reads were removed. For sites not called by JACUSA, we added read depth calculated by samtools pileup to reflect the sequence coverage at those positions. The editing rate for each genotype was calculated as the sum of edited reads for three replicates/total read depth for all three replicates. Sites required ≥ 50 read coverage in all samples (a combined read coverage of ≥ 50 for all genotypes was required) of the comparison and an editing rate of ≥ 0.01 ($\geq 1\%$) in the WT to be considered. See Dataset EV1.

Differential editing of known sites: Calling of differential editing in known sites across genotypes was performed using JACUSA 2.0.0-RC5 (Piechotta *et al*, 2017). Briefly, call-2 was used to determine the difference in editing level for all known sites (all replicates of genotype A vs. all replicates of genotype B). Duplicate reads were removed. Sites required ≥ 50 read coverage and an editing rate of ≥ 0.01 ($\geq 1\%$) to be considered. See Dataset EV1.

Annotation: Editing sites were annotated with gene and gene part (promoter, Exon, intron, 3' UTR or intergenic) using Goldmine (Bhasin & Ting, 2016). B1 and B2 SINE annotation (mm10) was from UCSC rmsk table (Meyer *et al*, 2013). Z-RNAs annotated using Z22-bound RNAs were identified by Zhang *et al*, 2022 (Zhang *et al*, 2022). See Dataset EV1.

Gene expression

Current study: Counts were determined by mapping trimmed reads using Salmon (v1.6.0) versus mm11 gencode vm28 (Patro *et al*, 2017). Salmon count data were processed using tximeta (Love *et al*, 2020), and summarised to gene using lengthScaledTPM. Normalisation, QC and filtering were performed in Degust (Powell, 2019). Genes were filtered (count > 1, min CPM > 1 in at least three samples) and differential expression was performed using edgeR-quasi-likelihood (Robinson *et al*, 2010). Each comparison (*Adar1*^{P195A/+} vs. WT, *Adar1*^{P195A/P195A} vs. WT, *Adar1*^{P195A/-} vs. WT and *Adar1*^{P195A/-} vs. *Adar1*^{P195A/P195A}) was performed separately. See Dataset EV2.

Heatmaps

Tidyheatmap (Mangiola & Papenfuss, 2020) was used to visualise datasets.

Gene set testing (QuSAGE analysis)

For gene set testing, Quantitative Set Analysis for Gene Expression (QuSAGE) (Yaari *et al*, 2013) was used with $n = 2^{18}$. The interferon-stimulated gene set was derived from Liu *et al* (2019) and the integrated stress response from supp file 1D of Wong *et al* (2019), combining the CLIC and manual curated lists. See Dataset EV2.

Statistical analysis

To determine statistical significance, Kaplan–Meier survival plots, log-rank tests, *t*-tests and ordinary one-way ANOVA tests were conducted in GraphPad Prism software version 9 (GraphPad; San Diego, CA, USA). Throughout this study, significance is indicated using the following convention: **P* < 0.05; ***P* < 0.01; ****P* < 0.001 and *****P* < 0.0001, and data are presented as mean \pm SEM. The number of samples used for each experiment is described in the figure panels or corresponding figure legends.

Data availability

Raw reads and processed data are available in GEO GSE220628 (<https://www.ncbi.nlm.nih.gov/geo/query/acc.cgi?acc=GSE220628>).

Expanded View for this article is available [online](#).

Acknowledgements

The authors would like to thank A Herbert, JB Li and Q Li for critical discussion and comment; E Tonkin for technical assistance; the Monash Genome Modification Platform (MGMP) at Monash University for the generation of the P195A mice; Monash Antibody Technology Facility (MATF) for purification of ADAR1 antibody from hybridomas; the Phenomics Australia Histopathology and Slide Scanning Service, University of Melbourne for histopathology on samples; and St. Vincent's Hospital BioResource's Centre for care of experimental animals. We thank R Dickins (Monash University) for shTp53-1224 vector and M Kamps (UC San Diego) for HOXA9 plasmids and Addgene for plasmid distribution. Schematic figures were made using [BioRender.com](#). The P195A mutant mice were produced via CRISPR/Cas9-mediated genome editing by the Monash Genome Modification Platform (MGMP), Monash University, as a node of Phenomics Australia. This study utilised the Phenomics Australia Histopathology and Slide Scanning Service, University of Melbourne. Phenomics Australia is supported by the Australian Government Department of Education through the National Collaborative Research Infrastructure Strategy, the Super Science Initiative and the Collaborative Research Infrastructure Scheme. This work was supported by the National Health and Medical Research Council (NHMRC; GNT1183553 to C.R.W. and J.H.F.; GNT1182453 to J.H.F.); a Melbourne Research Scholarship (to Z.L. from The University of Melbourne); J.H.F. is supported by a fellowship from 5point Foundation; and in part by the Victorian State Government Operational Infrastructure Support Scheme to St Vincent's Institute. The funders had no role in study design, data collection and analysis, decision to publish or preparation of the manuscript.

Author contributions

Zhen Liang: Conceptualization; formal analysis; investigation; visualization; writing – original draft; writing – review and editing. **Alistair M Chalk:** Formal analysis; funding acquisition; visualization; methodology; writing – review and editing. **Scott Taylor:** Investigation. **Ankita Goradia:** Investigation. **Jacki E Heraud-Farlow:** Conceptualization; supervision; funding acquisition; investigation; visualization; methodology; writing – original draft; project administration; writing – review and editing. **Carl R Walkley:** Conceptualization; supervision; funding acquisition; investigation; visualization; methodology; writing – original draft; project administration; writing – review and editing.

Disclosure and competing interests statement

The authors declare that they have no conflict of interest.

References

- Bajad P, Ebner F, Amman F, Szabo B, Kapoor U, Manjali G, Hildebrandt A, Jansiw MP, Jantsch MF (2020) An internal deletion of ADAR rescued by MAVS deficiency leads to a minute phenotype. *Nucleic Acids Res* 48: 3286–3303
- Bazak L, Haviv A, Barak M, Jacob-Hirsch J, Deng P, Zhang R, Isaacs FJ, Rechavi G, Li JB, Eisenberg E et al (2014) A-to-I RNA editing occurs at over a hundred million genomic sites, located in a majority of human genes. *Genome Res* 24: 365–376
- Bhasin JM, Ting AH (2016) Goldmine integrates information placing genomic ranges into meaningful biological contexts. *Nucleic Acids Res* 44: 5550–5556
- Chalk AM, Taylor S, Heraud-Farlow JE, Walkley CR (2019) The majority of A-to-I RNA editing is not required for mammalian homeostasis. *Genome Biol* 20: 268
- Chen S, Zhou Y, Chen Y, Gu J (2018) Fastp: an ultra-fast all-in-one FASTQ preprocessor. *Bioinformatics* 34: i884–i890
- Cho DS, Yang W, Lee JT, Shiekhattar R, Murray JM, Nishikura K (2003) Requirement of dimerization for RNA editing activity of adenosine deaminases acting on RNA. *J Biol Chem* 278: 17093–17102
- Chung H, Calis JJA, Wu X, Sun T, Yu Y, Sarbanes SL, Dao Thi VL, Shilvock AR, Hoffmann HH, Rosenberg BR et al (2018) Human ADAR1 prevents endogenous RNA from triggering translational shutdown. *Cell* 172: 811–824.e14
- Costa Cruz PH, Kato Y, Nakahama T, Shibuya T, Kawahara Y (2020) A comparative analysis of ADAR mutant mice reveals site-specific regulation of RNA editing. *RNA* 26: 454–469
- Crow YJ, Manel N (2015) Aicardi-Goutieres syndrome and the type I interferonopathies. *Nat Rev Immunol* 15: 429–440
- Dickins RA, Hemann MT, Zilfou JT, Simpson DR, Ibarra I, Hannon GJ, Lowe SW (2005) Probing tumor phenotypes using stable and regulated synthetic microRNA precursors. *Nat Genet* 37: 1289–1295
- Dickinson ME, Flenniken AM, Ji X, Teboul L, Wong MD, White JK, Meehan TF, Weninger WJ, Westerberg H, Adissu H et al (2016) High-throughput discovery of novel developmental phenotypes. *Nature* 537: 508–514
- Eisenberg E, Levanon EY (2018) A-to-I RNA editing – immune protector and transcriptome diversifier. *Nat Rev Genet* 19: 473–490
- Essers MA, Offner S, Blanco-Bose WE, Waibler Z, Kalinke U, Duchosal MA, Trumpp A (2009) IFN α activates dormant haematopoietic stem cells *in vivo*. *Nature* 458: 904–908
- Gabay O, Shoshan Y, Kopel E, Ben-Zvi U, Mann TD, Bressler N, Cohen-Fultheim R, Schaffer AA, Roth SH, Tzur Z et al (2022) Landscape of adenosine-to-inosine RNA recoding across human tissues. *Nat Commun* 13: 1184
- Gitlin L, Barchet W, Gilfillan S, Cella M, Beutler B, Flavell RA, Diamond MS, Colonna M (2006) Essential role of mda-5 in type I IFN responses to polyriboinosinic:polyribocytidylic acid and encephalomyocarditis picornavirus. *Proc Natl Acad Sci USA* 103: 8459–8464
- Guo X, Wiley CA, Steinman RA, Sheng Y, Ji B, Wang J, Zhang L, Wang T, Zenatai M, Billiar TR et al (2021) Aicardi-Goutieres syndrome-associated mutation at ADAR1 gene locus activates innate immune response in mouse brain. *J Neuroinflammation* 18: 169
- Hartner JC, Schmittwolf C, Kispert A, Muller AM, Higuchi M, Seeburg PH (2004) Liver disintegration in the mouse embryo caused by deficiency in the RNA-editing enzyme ADAR1. *J Biol Chem* 279: 4894–4902
- Hartner JC, Walkley CR, Lu J, Orkin SH (2009) ADAR1 is essential for the maintenance of hematopoiesis and suppression of interferon signaling. *Nat Immunol* 10: 109–115
- Heraud-Farlow JE, Chalk AM, Linder SE, Li Q, Taylor S, White JM, Pang L, Liddicoat BJ, Gupte A, Li JB et al (2017) Protein recoding by ADAR1-mediated RNA editing is not essential for normal development and homeostasis. *Genome Biol* 18: 166
- Herbert A (2020) Mendelian disease caused by variants affecting recognition of Z-DNA and Z-RNA by the Zalpha domain of the double-stranded RNA editing enzyme ADAR. *Eur J Hum Genet* 28: 114–117
- Herbert A (2021) To "Z" or not to "Z": Z-RNA, self-recognition, and the MDA5 helicase. *PLoS Genet* 17: e1009513
- Herbert A, Rich A (2001) The role of binding domains for dsRNA and Z-DNA in the *in vivo* editing of minimal substrates by ADAR1. *Proc Natl Acad Sci USA* 98: 12132–12137
- Herbert A, Lowenhaupt K, Spitzner J, Rich A (1995) Double-stranded RNA adenosine deaminase binds Z-DNA *in vitro*. *Nucleic Acids Symp Ser* 16–19
- Herbert A, Schade M, Lowenhaupt K, Alfken J, Schwartz T, Shlyakhtenko LS, Lyubchenko YL, Rich A (1998) The Zalpha domain from human ADAR1 binds to the Z-DNA conformer of many different sequences. *Nucleic Acids Res* 26: 3486–3493
- Higuchi M, Single FN, Kohler M, Sommer B, Sprengel R, Seeburg PH (1993) RNA editing of AMPA receptor subunit GluR-B: a base-paired intron-exon structure determines position and efficiency. *Cell* 75: 1361–1370
- Higuchi M, Maas S, Single FN, Hartner J, Rozov A, Burnashev N, Feldmeyer D, Sprengel R, Seeburg PH (2000) Point mutation in an AMPA receptor gene rescues lethality in mice deficient in the RNA-editing enzyme ADAR2. *Nature* 406: 78–81
- Hubbard NW, Ames JM, Maurano M, Chu LH, Somfleth KY, Gokhale NS, Werner M, Snyder JM, Lichauro K, Savan R et al (2022) ADAR1 mutation causes ZBP1-dependent immunopathology. *Nature* 607: 769–775
- Inoue M, Nakahama T, Yamasaki R, Shibuya T, Kim JI, Todo H, Xing Y, Kato Y, Morii E, Kawahara Y (2021) An Aicardi-Goutieres syndrome-causative point mutation in Adar1 gene invokes multiorgan inflammation and late-onset encephalopathy in mice. *J Immunol* 207: 3016–3027
- Ivanov A, Memczak S, Wyler E, Torti F, Porath HT, Orejuela MR, Piechotta M, Levanon EY, Landthaler M, Dieterich C et al (2015) Analysis of intron sequences reveals hallmarks of circular RNA biogenesis in animals. *Cell Rep* 10: 170–177
- Jiao H, Wachsmuth L, Kumari S, Schwarzer R, Lin J, Eren RO, Fisher A, Lane R, Young GR, Kassiotis G et al (2020) Z-nucleic-acid sensing triggers ZBP1-dependent necroptosis and inflammation. *Nature* 580: 391–395
- Jiao H, Wachsmuth L, Wolf S, Lohmann J, Nagata M, Kaya GG, Oikonomou N, Kondylis V, Rogg M, Diebold M et al (2022) ADAR1 averts fatal type I interferon induction by ZBP1. *Nature* 607: 776–783
- Kapoor U, Licht K, Amman F, Jakobi T, Martin D, Dieterich C, Jantsch MF (2020) ADAR-deficiency perturbs the global splicing landscape in mouse tissues. *Genome Res* 30: 1107–1118
- Karczewski KJ, Francioli LC, Tiao G, Cummings BB, Alfoldi J, Wang Q, Collins RL, Laricchia KM, Ganna A, Birnbaum DP et al (2020) The mutational constraint spectrum quantified from variation in 141,456 humans. *Nature* 581: 434–443
- Kawahara Y, Zinshteyn B, Chendrimada TP, Shiekhattar R, Nishikura K (2007) RNA editing of the microRNA-151 precursor blocks cleavage by the dicer-TRBP complex. *EMBO Rep* 8: 763–769
- Kim JI, Nakahama T, Yamasaki R, Costa Cruz PH, Vongpipatana T, Inoue M, Kanou N, Xing Y, Todo H, Shibuya T et al (2021) RNA editing at a limited number of sites is sufficient to prevent MDA5 activation in the mouse brain. *PLoS Genet* 17: e1009516

- Koehler HS, Feng Y, Mandal P, Mocarski ES (2020) Recognizing limits of Z-nucleic acid binding protein (ZBP1/DAI/DLM1) function. *FEBS J* 287: 4362–4369
- Levanon EY, Eisenberg E, Yelin R, Nemzer S, Hallegger M, Shemesh R, Fligelman ZY, Shoshan A, Pollock SR, Sztybel D et al (2004) Systematic identification of abundant A-to-I editing sites in the human transcriptome. *Nat Biotechnol* 22: 1001–1005
- Lev-Maor G, Sorek R, Levanon EY, Paz N, Eisenberg E, Ast G (2007) RNA-editing-mediated exon evolution. *Genome Biol* 8: R29
- Li JB, Levanon EY, Yoon JK, Aach J, Xie B, Leproust E, Zhang K, Gao Y, Church GM (2009) Genome-wide identification of human RNA editing sites by parallel DNA capturing and sequencing. *Science* 324: 1210–1213
- Liang Z, Walkley CR, Heraud-Farlow JE (2022) Generation of a new Adar1p150-/- mouse demonstrates isoform-specific roles in embryonic development and adult homeostasis. *bioRxiv* <https://doi.org/10.1101/2022.08.31.506069> [PREPRINT]
- Licht K, Kapoor U, Amman F, Picardi E, Martin D, Bajad P, Jantsch MF (2019) A high resolution A-to-I editing map in the mouse identifies editing events controlled by pre-mRNA splicing. *Genome Res* 29: 1453–1463
- Liddicoat BJ, Piskol R, Chalk AM, Ramaswami G, Higuchi M, Hartner JC, Li JB, Seeburg PH, Walkley CR (2015) RNA editing by ADAR1 prevents MDA5 sensing of endogenous dsRNA as nonself. *Science* 349: 1115–1120
- Liddicoat BJ, Chalk AM, Walkley CR (2016a) ADAR1, inosine and the immune sensing system: distinguishing self from non-self. *Wiley Interdiscip Rev RNA* 7: 157–172
- Liddicoat BJ, Hartner JC, Piskol R, Ramaswami G, Chalk AM, Kingsley PD, Sankaran VG, Wall M, Purton LE, Seeburg PH et al (2016b) Adenosine-to-inosine RNA editing by ADAR1 is essential for normal murine erythropoiesis. *Exp Hematol* 44: 947–963
- Liu H, Golji J, Brodeur LK, Chung FS, Chen JT, deBeaumont RS, Bullock CP, Jones MD, Kerr G, Li L et al (2019) Tumor-derived IFN triggers chronic pathway agonism and sensitivity to ADAR loss. *Nat Med* 25: 95–102
- Livingston JH, Lin JP, Dale RC, Gill D, Brogan P, Munnich A, Kurian MA, Gonzalez-Martinez V, De Goede CG, Falconer A et al (2014) A type I interferon signature identifies bilateral striatal necrosis due to mutations in ADAR1. *J Med Genet* 51: 76–82
- Love MI, Sonesson C, Hickey PF, Johnson LK, Pierce NT, Shepherd L, Morgan M, Patro R (2020) Tximeta: reference sequence checksums for provenance identification in RNA-seq. *PLoS Comput Biol* 16: e1007664
- Mangiola S, Papefuss AT (2020) tidyHeatmap: an R package for modular heatmap production based on tidy principles. *J Open Source Softw* 5: 2472
- Mannion NM, Greenwood SM, Young R, Cox S, Brindle J, Read D, Nellaker C, Vesely C, Ponting CP, McLaughlin PJ et al (2014) The RNA-editing enzyme ADAR1 controls innate immune responses to RNA. *Cell Rep* 9: 1482–1494
- Maurano M, Snyder JM, Connelly C, Henao-Mejia J, Sidrauski C, Stetson DB (2021) Protein kinase R and the integrated stress response drive immunopathology caused by mutations in the RNA deaminase ADAR1. *Immunity* 54: 1948–1960.e5
- Meyer LR, Zweig AS, Hinrichs AS, Karolchik D, Kuhn RM, Wong M, Sloan CA, Rosenbloom KR, Roe G, Rhead B et al (2013) The UCSC genome browser database: extensions and updates 2013. *Nucleic Acids Res* 41: D64–D69
- Nakahama T, Kawahara Y (2021) Deciphering the biological significance of ADAR1-Z-RNA interactions. *Int J Mol Sci* 22: 11435
- Nakahama T, Kato Y, Shibuya T, Inoue M, Kim JI, Vongpipatana T, Todo H, Xing Y, Kawahara Y (2021) Mutations in the adenosine deaminase ADAR1 that prevent endogenous Z-RNA binding induce Aicardi-Goutieres-syndrome-like encephalopathy. *Immunity* 54: 1976–1988.e7
- Newton K, Wickliffe KE, Maltzman A, Dugger DL, Strasser A, Pham VC, Lill JR, Roose-Girma M, Warming S, Solon M et al (2016) RIPK1 inhibits ZBP1-driven necroptosis during development. *Nature* 540: 129–133
- Patro R, Duggal G, Love MI, Irizarry RA, Kingsford C (2017) Salmon provides fast and bias-aware quantification of transcript expression. *Nat Methods* 14: 417–419
- Pestal K, Funk CC, Snyder JM, Price ND, Treuting PM, Stetson DB (2015) Isoforms of RNA-editing enzyme ADAR1 independently control nucleic acid sensor MDA5-driven autoimmunity and multi-organ development. *Immunity* 43: 933–944
- Pfaller CK, Donohue RC, Nersisyan S, Brodsky L, Cattaneo R (2018) Extensive editing of cellular and viral double-stranded RNA structures accounts for innate immunity suppression and the proviral activity of ADAR1p150. *PLoS Biol* 16: e2006577
- Picardi E, Manzari C, Mastropasqua F, Aiello I, D'Erchia AM, Pesole G (2015) Profiling RNA editing in human tissues: towards the inosinome atlas. *Sci Rep* 5: 14941
- Piechotta M, Wyler E, Ohler U, Landthaler M, Dieterich C (2017) JACUSA: site-specific identification of RNA editing events from replicate sequencing data. *BMC Bioinformatics* 18: 7
- Pinto Y, Cohen HY, Levanon EY (2014) Mammalian conserved ADAR targets comprise only a small fragment of the human editosome. *Genome Biol* 15: R5
- Powell D (2019) drpowell/degust 4.1.1. *Zenodo*.
- Ramaswami G, Li JB (2014) RADAR: a rigorously annotated database of A-to-I RNA editing. *Nucleic Acids Res* 42: D109–D113
- Ramaswami G, Zhang R, Piskol R, Keegan LP, Deng P, O'Connell MA, Li JB (2013) Identifying RNA editing sites using RNA sequencing data alone. *Nat Methods* 10: 128–132
- de Reuver R, Dierick E, Wiernicki B, Staes K, Seys L, De Meester E, Muylderms T, Botzki A, Lambrecht BN, Van Nieuwerburgh F et al (2021) ADAR1 interaction with Z-RNA promotes editing of endogenous double-stranded RNA and prevents MDA5-dependent immune activation. *Cell Rep* 36: 109500
- Rice GI, Kasher PR, Forte GM, Mannion NM, Greenwood SM, Szykiewicz M, Dickerson JE, Bhaskar SS, Zampini M, Briggs TA et al (2012) Mutations in ADAR1 cause Aicardi-Goutieres syndrome associated with a type I interferon signature. *Nat Genet* 44: 1243–1248
- Rice GI, Kitabayashi N, Barth M, Briggs TA, Burton ACE, Carpanelli ML, Cerisola AM, Colson C, Dale RC, Danti FR et al (2017) Genetic, phenotypic, and interferon biomarker status in ADAR1-related neurological disease. *Neuropediatrics* 48: 166–184
- Robinson MD, McCarthy DJ, Smyth GK (2010) edgeR: a Bioconductor package for differential expression analysis of digital gene expression data. *Bioinformatics* 26: 139–140
- Roth SH, Levanon EY, Eisenberg E (2019) Genome-wide quantification of ADAR adenosine-to-inosine RNA editing activity. *Nat Methods* 16: 1131–1138
- Schwartz T, Rould MA, Lowenhaupt K, Herbert A, Rich A (1999) Crystal structure of the Z-alpha domain of the human editing enzyme ADAR1 bound to left-handed Z-DNA. *Science* 284: 1841–1845
- Shoshan E, Mobley AK, Braeuer RR, Kamiya T, Huang L, Vasquez ME, Salameh A, Lee HJ, Kim SJ, Ivan C et al (2015) Reduced adenosine-to-inosine miR-455-5p editing promotes melanoma growth and metastasis. *Nat Cell Biol* 17: 311–321
- Singbrant S, Russell MR, Jovic T, Liddicoat B, Izon DJ, Purton LE, Sims NA, Martin TJ, Sankaran VG, Walkley CR (2011) Erythropoietin couples

- erythropoiesis, B-lymphopoiesis, and bone homeostasis within the bone marrow microenvironment. *Blood* 117: 5631–5642
- Smeets MF, DeLuca E, Wall M, Quach JM, Chalk AM, Deans AJ, Heierhorst J, Purton LE, Izon DJ, Walkley CR (2014) The Rothmund-Thomson syndrome helicase RECQL4 is essential for hematopoiesis. *J Clin Invest* 124: 3551–3565
- Solomon O, Oren S, Safran M, Deshet-Unger N, Akiva P, Jacob-Hirsch J, Cesarkas K, Kabesa R, Amariglio N, Unger R et al (2013) Global regulation of alternative splicing by adenosine deaminase acting on RNA (ADAR). *RNA* 19: 591–604
- Solomon O, Di Segni A, Cesarkas K, Porath HT, Marcu-Malina V, Mizrahi O, Stern-Ginossar N, Kol N, Farage-Barhom S, Glick-Saar E et al (2017) RNA editing by ADAR1 leads to context-dependent transcriptome-wide changes in RNA secondary structure. *Nat Commun* 8: 1440
- Steinman RA, Wang Q (2011) ADAR1 isoform involvement in embryonic lethality. *Proc Natl Acad Sci USA* 108: E199; author reply E200
- Stellos K, Gatsiou A, Stamatelopoulou K, Perisic Matic L, John D, Lunella FF, Jae N, Rossbach O, Amrhein C, Sigala F et al (2016) Adenosine-to-inosine RNA editing controls cathepsin S expression in atherosclerosis by enabling HuR-mediated post-transcriptional regulation. *Nat Med* 22: 1140–1150
- Subramani VK, Kim D, Yun K, Kim KK (2016) Structural and functional studies of a large winged Z-DNA-binding domain of Danio rerio protein kinase PKZ. *FEBS Lett* 590: 2275–2285
- Sun T, Li Q, Geisinger JM, Hu S-B, Fan B, Su S, Tsui W, Guo H, Ma J, Li JB (2022) A small subset of cytosolic dsRNAs must be edited by ADAR1 to evade MDA5-mediated autoimmunity. *bioRxiv* <https://doi.org/10.1101/2022.08.29.505707> [PREPRINT]
- Tan MH, Li Q, Shanmugam R, Piskol R, Kohler J, Young AN, Liu KI, Zhang R, Ramaswami G, Ariyoshi K et al (2017) Dynamic landscape and regulation of RNA editing in mammals. *Nature* 550: 249–254
- Tang Q, Rigby RE, Young GR, Hvidt AK, Davis T, Tan TK, Bridgeman A, Townsend AR, Kassiotis G, Rehwinkel J (2021) Adenosine-to-inosine editing of endogenous Z-form RNA by the deaminase ADAR1 prevents spontaneous MAVS-dependent type I interferon responses. *Immunity* 54: 1961–1975.e5
- Valente L, Nishikura K (2007) RNA binding-independent dimerization of adenosine deaminases acting on RNA and dominant negative effects of nonfunctional subunits on dimer functions. *J Biol Chem* 282: 16054–16061
- Ventura A, Kirsch DG, McLaughlin ME, Tuveson DA, Grimm J, Lintault L, Newman J, Reczek EE, Weissleder R, Jacks T (2007) Restoration of p53 function leads to tumour regression *in vivo*. *Nature* 445: 661–665
- Walkley CR, Li JB (2017) Rewriting the transcriptome: adenosine-to-inosine RNA editing by ADARs. *Genome Biol* 18: 205
- Wang Q, Miyakoda M, Yang W, Khillan J, Stachura DL, Weiss MJ, Nishikura K (2004) Stress-induced apoptosis associated with null mutation of ADAR1 RNA editing deaminase gene. *J Biol Chem* 279: 4952–4961
- Wang GG, Calvo KR, Pasillas MP, Sykes DB, Hacker H, Kamps MP (2006) Quantitative production of macrophages or neutrophils ex vivo using conditional Hoxb8. *Nat Methods* 3: 287–293
- Ward SV, George CX, Welch MJ, Liou LY, Hahm B, Lewicki H, de la Torre JC, Samuel CE, Oldstone MB (2011) RNA editing enzyme adenosine deaminase is a restriction factor for controlling measles virus replication that also is required for embryogenesis. *Proc Natl Acad Sci USA* 108: 331–336
- Wong YL, LeBon L, Basso AM, Kohlhaas KL, Nikkel AL, Robb HM, Donnelly-Roberts DL, Prakash J, Swensen AM, Rubinstein ND et al (2019) eIF2B activator prevents neurological defects caused by a chronic integrated stress response. *Elife* 8: e42940
- Yaari G, Bolen CR, Thakar J, Kleinstein SH (2013) Quantitative set analysis for gene expression: a method to quantify gene set differential expression including gene-gene correlations. *Nucleic Acids Res* 41: e170
- Zhang R, Li X, Ramaswami G, Smith KS, Turecki G, Montgomery SB, Li JB (2014) Quantifying RNA allelic ratios by microfluidic multiplex PCR and sequencing. *Nat Methods* 11: 51–54
- Zhang T, Yin C, Boyd DF, Quarato G, Ingram JP, Shubina M, Ragan KB, Ishizuka T, Crawford JC, Tummers B et al (2020) Influenza virus Z-RNAs induce ZBP1-mediated necroptosis. *Cell* 180: 1115–1129.e13
- Zhang T, Yin C, Fedorov A, Qiao L, Bao H, Beknazarov N, Wang S, Gautam A, Williams RM, Crawford JC et al (2022) ADAR1 masks the cancer immunotherapeutic promise of ZBP1-driven necroptosis. *Nature* 606: 594–602